UNCLASSIFIED

AD **295 659**

Reproduced
by the

ARMED SERVICES TECHNICAL INFORMATION AGENCY
ARLINGTON HALL STATION
ARLINGTON 12, VIRGINIA

UNCLASSIFIED

295 659

AFCRL-62-927

295659

RADIO CORPORATION OF AMERICA
RCA LABORATORIES

SCIENTIFIC REPORT NO. 3

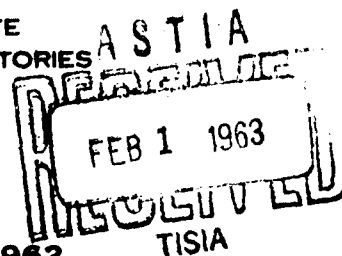## MAXIMIZING THE PERFORMANCE
OF PHOTOCONDUCTORS

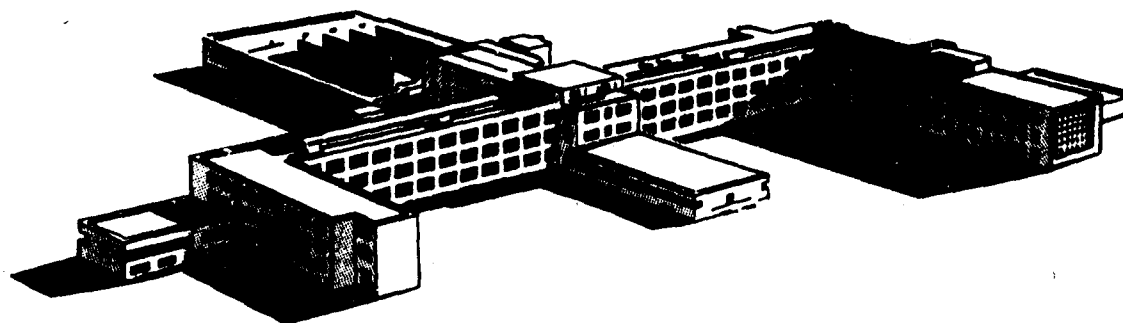CONTRACT NO. AF19(604)8353
PROJECT NO. 4608 - TASK NO. 460804

PREPARED FOR

ELECTRONICS RESEARCH DIRECTORATE
AIR FORCE CAMBRIDGE RESEARCH LABORATORIES
OFFICE OF AEROSPACE RESEARCH
UNITED STATES AIR FORCE
BEDFORD, MASSACHUSETTS

ASTIA

FEB 1 1963

TISIA

REPORT DATE: NOVEMBER 14, 1962

DAVID SARNOFF RESEARCH CENTER
PRINCETON, NEW JERSEY

SCIENTIFIC REPORT NO. 3

Covering the Period

March 15, 1962 – September 15, 1962

Report Date: November 14, 1962

MAXIMIZING THE PERFORMANCE

OF PHOTOCONDUCTORS

CONTRACT NO. AF19(604)8353
PROJECT NO. 4608 – TASK NO. 460804

RADIO CORPORATION OF AMERICA
RCA LABORATORIES
PRINCETON, NEW JERSEY

Work Done by: W. M. Anderson

R. H. Bube (until 6/15/62)

A. B. Dreeben

J. Dresner

E. L. Lind (until 5/1/62)

P. Mark

Report Edited by: J. Dresner, Project Supervisor

TABLE OF CONTENTS

TABLE OF CONTENTS (Continued)

ABSTRACT

A general discussion of the problems of charge transport and contacts to wide band gap materials is given, followed by a review of the applicable experimental techniques.

The interpretation of Hall effect measurements in insulators and the related experimental problems are discussed in detail. The existing apparatus has been modified to permit measurements on samples having a resistance as high as 10^{12} ohms. A sample of amorphous selenium containing a large number of artificially introduced crystalline inclusions has been measured. This material yielded an n-type signal with a mobility of approximately 0.2 $cm^2 v^{-1} s^{-1}$. This unexpected result suggests that microcrystalline inclusions may constitute the sensitizing centers in amorphous selenium photoconductors.

A "time-of-flight" method for studying carrier transport in insulators is reviewed. This consists of a measurement of the transit time of injected excess carriers flowing under space charge limitation. The details of the method are outlined and the experimental limitations are examined. It is shown that carrier transport in any insulator may be investigated with this technique, provided that ohmic contact formation (either transient or steady state) is possible and that trapping is not too severe.

A general analysis of unipolar steady state space charge limited currents in insulators with non-planar electrode geometries is presented. The treatment encompasses collectively the following cases: trap free, single shallow trap level and exponential trap distribution, each for the plane parallel, cylindrical and hemispherical (point contact) electrode configurations. It is shown that current rectification occurs for the non-planar electrode configuration and that the magnitude of the rectification ratios depend both on the details of the electrode geometry and on the energy distribution of trapping states.

The electrical properties of the arsonium salt of tetracyanoquinodimethane (TCNQ) are examined in a preliminary effort to determine the contact properties of this material. It is concluded that this material behaves as a p-type semiconductor with promising application as an injecting contact to insulators.

Cubic cadmium sulfide was prepared by decomposition of cadmium mercaptide. Photoconductivity spectral response indicates a band gap of about 2.1 ev, i.e., about 0.3 ev smaller than the band gap of hexagonal cadmium sulfide.

Large boules of CdS with silver and gold impurities have been prepared by sublimation. Gold appears to accelerate the growth process. Some evidence for p-type conductivity in a CdS:Cu boule was obtained. The orientation of the c-axis in a large number of boules was determined and found to vary between 5-70° with respect to the growth axis. The pure CdS boules continue to show high conductivity, but one sample contained a high resistivity region. Cubic CdS has been prepared and its photoconductivity measured.

Crystals of hexagonal Se up to $2 \times 5 \times 0.4$ mm have been grown by sublimation in vacuo.

A Bridgman furnace has been constructed for growing crystals of organic compounds from the melt. Crystals of anthracene have been grown from solution.

LIST OF FIGURES

LIST OF TABLES

I. INTRODUCTION

The work of the last quarter differs from the previous portion of this contract which dealt mainly with the study of criteria leading to high photoconductive performance and the synthesis of photoconductive crystals. The emphasis has now shifted to a more general study of contacts and charge transport in wide band gap materials. This report begins with a statement of our general philosophy on the subject followed by a review of the experimental techniques applicable to these materials. It then describes our first experiments in this field dealing with contacts to crystals of the organic charge-transfer complex TCNQ and with measurements of the Hall effect in vitreous Se. Measurements of photoconductivity in the cubic phase of CdS are also described. Finally, progress in the preparation of crystals for this work will be discussed.

A first list of materials suitable for this investigation might include all crystalline semiconductors with a band gap greater than that of GaAs (E_g = 1.6 ev) as well as many organic molecular crystals and amorphous semiconductors, with primary interest on materials with E_g > 2.5 ev. Such a list is quickly reduced by practical considerations. While the detailed characteristics desired in a semiconductor depend on the particular application, general criteria can be stated for selecting materials with a reasonable probability of technical usefulness. Since the performance of many devices improves with the drift mobility (e.g. diodes, transistors, photocells) one would require a Hall mobility $\mu \geq 10 \ cm^2v^{-1}s^{-1}$ together with a minimum of deep trapping states. One should be able to vary the conductivity and carrier type in a controlled manner and there should exist contacts which can supply freely at least one type of carrier. Few of the wide band gap materials studied to date meet more than one of these requirements. *The almost universally encountered difficulty is that of making good contact to the material.* With the exception of a few substances which can be doped to give a high conductivity, such as TiO_2 or diamond, one does not generally know how to make ohmic contact to insulators. Some metallic ohmic contacts are known, such as In or Ga for CdS and ZnS, or Te for holes in Se. It has recently been discovered that solutions of strongly oxydizing ions (I_3-, Ce_4+) can serve as ohmic contacts for holes in some organic insulators[1,2,3] thus making these materials accessible to measurement. An "ohmic" contact can also be generated in some cases by illumination of the contact with strongly absorbed light, but the density of free carriers generated is limited. It is clear that a study of the mechanisms of carrier injection in insulators and a search for ohmic contacts to new materials must form a major part of our program.

Most previous studies of insulators have been limited to the measurement of dark- and photocurrents, often as function of temperature, in an attempt to establish correlations between thermal "activation energies" and the optical properties of the material. In some cases, the lifetime of free carriers has been estimated from measurements of luminescence and photoconductivity, while the density and energy distribution of traps have been obtained from glow curves and thermally stimulated currents. However, a more thorough understanding of insulators requires a knowledge of the transport parameters and of the actual mechanism of charge transport. In conventional semiconductors, this data is commonly obtained from measurements of the Hall effect, thermoelectric power and magneto-optic effects. The first two measurements yield the density and mobility of the carriers and can be applied to insulators, although with some difficulty. The Hall effect is particularly important, since from the temperature dependence of the mobility, one may be able to differentiate between the various models for charge transport in insulators. This will be discussed in more detail below. Magneto-optic effects yield effective-masses of carriers and thus information about the topology of the bands in cases where band models are applicable. However, they cannot be applied to most insulators. The requirement for cyclotron resonance, $B\mu > 1$, leading to mobilities in excess of 2000 cm^{2}v^{-1}s^{-1} for a field of 50,000 gauss can hardly be satisfied. The Faraday effect has been used to estimate effective-masses in materials of low mobility[4] but the interpretation of the results are of questionable validity for insulators, where the free carrier density is low.

In substances to which ohmic contact can be made, a useful technique is the study of injected excess carriers. When their density exceeds that of thermally generated carriers, the current becomes space-charge-limited (S.C.L.C.). From the dependence of the steady-state S.C.L.C. with applied voltage as well as with sample thickness, the energy spectrum of trapping states in the forbidden gap can be obtained, while their concentration is obtainable from the temperature dependence of the S.C.L.C. This type of measurement has been performed on many insulators; a recent review of the subject may be found in reference 5. The transient S.C.L.C. generated upon the application of a voltage step to the sample[6,7], or upon flash illumination of an electrode[8], has recently been investigated. This method yields the microscopic mobility of carriers by what is essentially a time-of-flight measurement, and is most useful in materials of low mobility, thus complementing the Hall effect. This method requires only that the contacts be able to deliver a current for a short time, rather than be truly ohmic. It can also yield the conductivity for insulators where good contacts do not exist[9]. Because of its potential importance in this field, the method of transient S.C.L.C. will be described in detail below.

2

II. HALL EFFECT IN INSULATORS

1. GENERAL CONSIDERATIONS

The primary data which can be obtained from measurements of the Hall effect are the free carrier concentration and the mobility μ. The method is then useful for selecting materials for further study; in addition, one hopes to distinguish between the various mechanisms of charge transport by studying the temperature dependence of μ, which is a crucial problem in insulator physics. In cases where simple band theory applies, one expects μ to vary with temperature as T^{-a}, where a is close to and somewhat larger than the value 1.5, calculated for acoustical scattering by the lattice. In some materials, μ is found to vary exponentially with T. This has been explained in terms of "wavy bands" or "hopping" models, where the carriers must acquire sufficient thermal energy to pass over potential barriers between the lattice sites[10]. In other cases, μ varies linearly with T, which is characteristic of a model where the carriers tunnel through these barriers[11]. The temperature enters in such a tunneling calculation through thermal fluctuations in the shape of the potential barriers. The last two models are thought to be especially applicable to molecular crystals, where the process determining the rate of charge transport is the transfer from one molecule to the next rather than motion along a chain or ring molecule. In view of the present state of the theory, caution must be exercised in interpreting the Hall effect data for these cases. It is not always clear precisely what carrier property is measured by the experiment, since, from the classic standpoint, the electron is subject to Lorentz forces only during the time it is actually "hopping." A recent quantum mechanical calculation[12] suggests that in this model, the sign of the Hall voltage is a property of the geometrical arrangement of the lattice and is determined by the number of nearest neighboring sites to which the carrier can make a transition. Similar considerations will undoubtedly have to be applied to the tunneling model, where the application of the magnetic field may change the transition probabilities.

2. EXPERIMENTAL PROBLEMS

For this study, it is desirable to be able to measure the Hall effect in samples with resistances as high as 10^{12} ohms for μ as low as 0.1 cm^{2}v^{-1}s^{-1}. The high resistances under consideration make AC methods inapplicable, so we shall limit the discussion to the DC method, and to the problems peculiar to its use on insulating materials.

3

To a first approximation the magnitude of the Hall signal is independent of the conductivity of the sample as long as the Debye length is small compared to its dimensions, a condition easily satisfied for samples of millimeter size. Neglecting the geometrical correction factors to make an order-of-magnitude calculation, we obtain for a square electrode configuration

$$V_h = \mu B V_x \times 10^{-8}$$

where μ is the mobility (cgs), B the magnetic field in gauss and V_x the applied longitudinal voltage. For $\mu = 0.1 \text{ cm}^2\text{v}^{-1}\text{s}^{-1}$ and a typical field of 5000 gauss, we obtain a signal V_h of 5 mV for $V_x = 1000$ volts. Whether such a signal is in fact measurable depends on the resistivity of the sample, the bandwidth of the detecting circuit and the noise level. A first limit on the magnitude of signal obtainable is set by the longitudinal voltage V_x, since all leakage currents in the apparatus must be kept small compared to the sample current, and leakage currents tend to increase as V^n, where usually $n > 2$. It is generally not practicable to keep the leakage resistances much above 10^{14} ohms, even for $V_x \sim 100$ volts. Since the input capacitance of the detecting circuit cannot be made much smaller than 100 pF, the response time upon application of the magnetic field may be as long as 100 seconds, thus making measurements difficult in the presence of drifts (see below). The response time can be reduced by using a lower input resistance for the detector, although this reduces the signal voltage and necessitate making a separate measurement of the interelectrode resistance of the sample in order to calculate V_h. This method has been used successfully to measure μ on crystals of metal-free phtalocyanine with a resistance of 10^{14} ohms[13]. Thermal noise in the sample poses a minor problem since for a resistance of $10^{12}\Omega$ and a detector bandwidth of 1 cps the open circuit noise would be approximately 0.2 mV at 300°K, or 5% of the expected signal. Other sources of noise are created by non-ohmic contacts or by barriers in polycrystalline samples. The magnitude of this noise voltage is difficult to estimate, but is is often large enough to make measurements very difficult. When the noise is not larger than the signal to be measured, its effect can be averaged out by graphical integration.

The misalignment of the Hall probes presents special difficulties in measuring insulators. A method of compensating the misalignment signal without destroying the high impedance of the input circuit was described in Report No. 2. However, if the sample is very resistive, as in the example given above, a misalignment of 0.1% in the probes (or in the shape of the equipotentials) gives a background signal of 1 volt, which is three orders larger than the signal to be measured. This misalignment voltage must then not drift more than 0.1% in the time necessary to make a measurement. The principal sources of drift are current changes due to slow trap-filling and to temperature variations. The latter are

important in wide band gap materials, where the activation energy may be large. Spatial temperature gradients can also cause difficulties. The thermoelectric power is given by (for the simplest band model)

$$\Theta = -\frac{k}{e} \left(2 - \frac{E_f}{kT}\right)$$

where e is the electronic charge, k the Bolzmann constant and E_f the Fermi energy. In a material where the resistivity is $10^{10} \Omega$-cm, with $\mu = 0.1$ cm^{2}v^{-1}s^{-1}, the Fermi level is located about 0.6 ev from the band edge at 300°K, leading to a value for $\Theta \sim 2$ mV/°K, again of the same magnitude as the signal to be measured. Special precautions must then be taken to insure isothermal conditions. The other thermo-magneto-galvanic effects (Ettingshausen, Nernst and Righi-Leduc) which appear in the presence of temperature gradients vary as μ, and are small compared to the Seebeck effect, except in materials with very high mobilities.

Another effect to be considered is magnetoresistance. In a homogeneous sample, the potential distribution is not affected by magnetoresistance and the effect would not interfere with the Hall signal. However, an inhomogeneously distributed magnetoresistance would change the probe potentials. The change in the conductivity due to the spread in carrier velocities can easily be calculated to be negligible for all but materials with very high mobilities. When it occurs, the spurious signal generated by it can easily be separated from the Hall voltage, since it is independent of the direction of the magnetic field. If the sample contains regions varying in resistivity, spatial variations in Hall voltage will distort the lines of current flow.* This entails a dissipation which increases the resistance without limit as the magnetic field increases[14]. This is essentially the same effect which causes anomalously large magnetoresistances due to shorting of the Hall signal near the electrodes. This effect has been observed on an amorphous Se sample rendered inhomogeneous by heat treatment, as described below.

The Hall apparatus described in Report No. 2 was capable of measuring samples with an interelectrode resistance $R \leq 10^9 \Omega$. This apparatus has been re-wired with Teflon insulation, so that all leakage resistances are normally greater than $5 \times 10^{13} \Omega$. An additional electrometer has been incorporated in the circuit for measuring small currents through the sample. The helium flow system previously used to vary the sample temperature cannot be used on the more resistive materials since it does not provide a sufficiently isothermal ambient. Furthermore, the gas tends to pick up charges from the insulator surfaces which can be deposited on the sample. In the Se sample measured, the noise was found to decrease considerably upon interruption of the He flow.

*(Although the average Hall signal is independent of the bulk conductivity of the sample, the local Hall field depends on the local current density.)

3. MEASUREMENTS ON AMORPHOUS SELENIUM

This section presents the results of our first Hall effect measurements on insulators. Selenium was chosen because it presents an interesting problem of conduction in a wide-band-gap semiconductor. This element exists in several allotropic forms of which two are of interest for this research. The gray hexagonal crystalline form is an intrinsic p-type semiconductor with a band gap of 1.8 ev. Large crystals of this material would be of technical interest, especially as a wide band gap hole emitter. Measurements of the Hall mobility to date[15] show $\mu = 0.14$ $cm^2v^{-1}s^{-1}$. As discussed below, there is a possibility that this value is limited by the quality of the crystal and that it may be intrinsically much higher. An attempt is now in progress to grow large carefully annealed crystals of hexagonal Se and is described in Section VII of this report. The other allotrope of interest here is vitreous Se with an optical band gap of 2.8 ev. This material is usually prepared by vacuum deposition and has normally a dark resistivity larger than 10^{12} Ω-cm. In neither of these two forms is the conductivity process well understood, and the literature on the subject is extensive. Some of the recent work of interest to this project is described in references 16 to 19. Spear[17] measured the drift mobility of holes generated at one surface of a thin film of vitreous Se by a pulsed electron beam, obtaining $\mu_{drift} = 0.14$ $cm^2v^{-1}s^{-1}$. This drift mobility was found to vary exponentially with temperature, with an activation energy of approximately 0.13 ev/kT, the same as that measured in the hexagonal form. The close agreement suggests that the mechanisms controlling the hole mobility in the two forms of Se are identical. A reasonable interpretation of this exponential dependence is that the drift mobility is trap-controlled[20], which leads Spear to calculate a microscopic mobility of 60 $cm^2v^{-1}s^{-1}$. Such a high mobility, unusual in an amorphous wide-band-gap semiconductor, should be detectable by Hall effect and thermoelectric power measurements. Values of μ as high as 30 $cm^2v^{-1}s^{-1}$ have been inferred from thermoelectric power measurements for both hexagonal crystals and liquid Se[21]. It is of interest therefore to attempt a Hall measurement on amorphous Se in order to verify this hypothesis. Should the Hall mobility in fact be so high in the disordered amorphous form, it is difficult to understand the low value measured in the well ordered hexagonal form unless the latter is limited by dislocations in the crystal.

A sample of vitreous Se is shown in Fig. II-1. Both the Au electrode structure and the Se film were deposited by evaporation on a glass substrate. The size of the sample (2 mm square) was chosen to give the best compromise between the desired low inter-electrode resistance and the accuracy presently obtainable in positioning the electrodes. The thickness of the layer was limited to 5μ in order to permit nearly homogeneous photo-excitation of the sample, since the diffusion length of holes is about 10μ[22]. Although Au

2mm
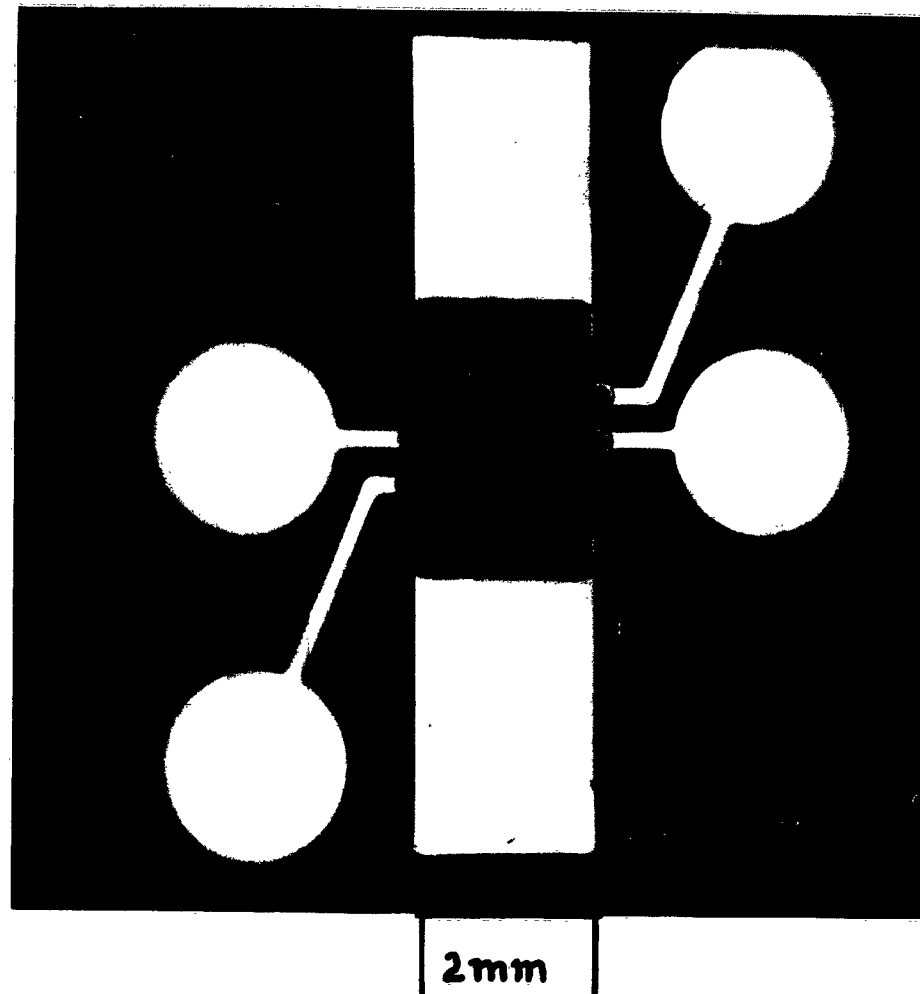
FIG. II-1.

contacts had previously been used with success[16], the contacts on this sample generated too high a noise level to make measurements possible, and attempts to form the contacts by applying 600 volts to them were unsuccessful. The work of Lanyon and Spear[18] indicated that Te contacts can be formed in this manner and samples of this type have been prepared, although they could not be measured in time for inclusion in this report.

In order to test the measuring method, the sample with Au electrodes (Se 285) was treated by heating for one hour at 80°C with 600 volts applied between the current contacts. This process reduced the dark resistance of the sample from 2×10^{14} ohms to 10^{12} ohms, and formed a large number of crystalline inclusions of the hexagonal form a few microns in size in the glassy matrix. These crystallites appear to form preferentially along the lines of force of the electric field applied during the heat treatment. Since the hexagonal phase is much more conductive than the vitreous phase, the crystallite ends are regions of high fields and high mechanical stresses. The latter are known to enhance crystallization in Se[23]. Such a process would result in the creation of conducting filaments. While the crystallites appear to be isolated from each other under microscopic observation, it is possible that they are electrically connected by lines of microcrystallites.

Under illumination, the sample resistance was reduced to approximately 10^{11} Ω. While the noise in the Hall signal is still considerable, it was sufficiently reduced to make a measurement possible. A sample of the data is shown in Fig. II-2, where B^+ and B^- indicate the polarity of the magnetic field. The noise was averaged out by graphical integration, yielding for this particular run signals of 1.04 and 2.32 mV of the same sign for the two directions of magnetic field. Five runs were taken at 22°C under different illumination conditions, yielding similar results, the deflection being always larger for the n-type signal. The calculated mobilities for electrons ranged from 0.05 to 0.46 $cm^2v^{-1}s^{-1}$. The measurement of an n-type conductivity under illumination in this type of sample is a new and unexpected result. It suggests that in the photoconductive amorphous Se, the sensitizing centers are microcrystalline inclusions of the hexagonal phase formed by nucleation during the evaporation of the sample. In order to explain the long-wavelength-quenching and the negative photoconductivity in amorphous Se, one must postulate that minority-carriers (electrons) can be optically released from these centers[16]. In the present sample, where the density of crystallites is much higher, this process may be dominant. This hypothesis is now being tested more thoroughly.

The identical sign of the signal upon reversing the magnetic field suggests the presence of an inhomogeneous magnetoresistance. Figure II-3 shows the change in current through the sample under constant applied voltage as a function of the magnetic induction B,

8

Se 285 — 22°C

BLUE ILLUMINATION (5–61 FILTER)

FIG. II-2

HALL PROBE VOLTAGE(mV)

TIME(MINUTES)

9
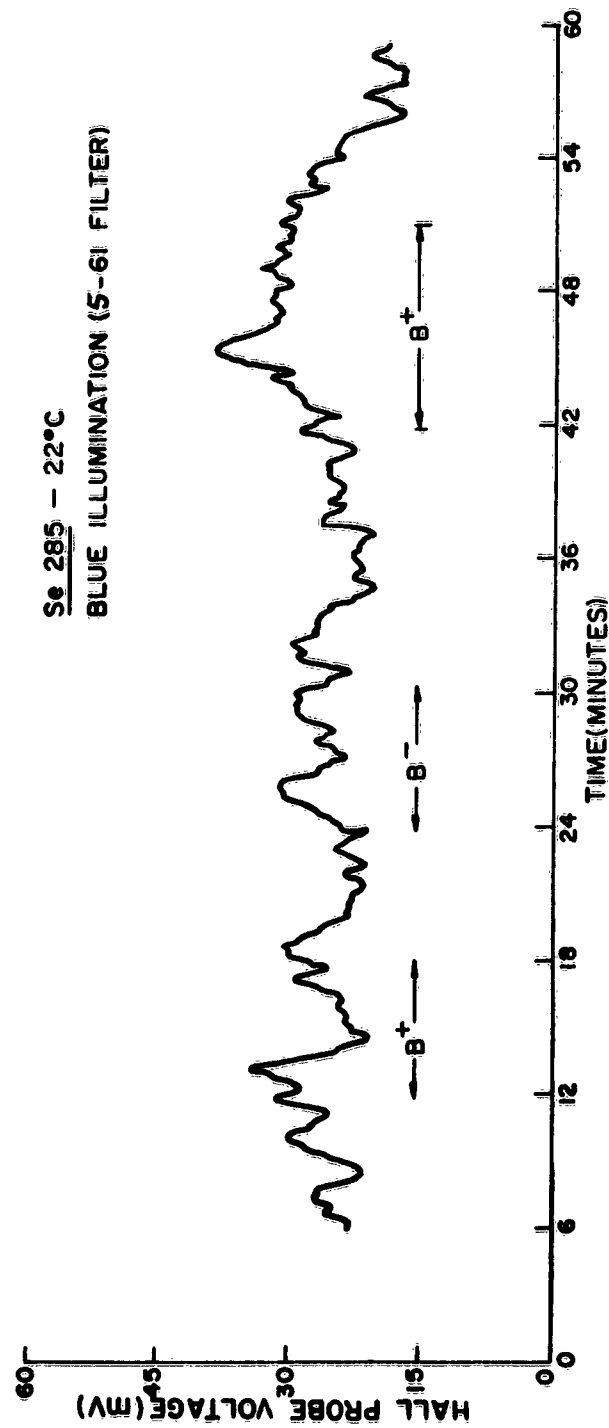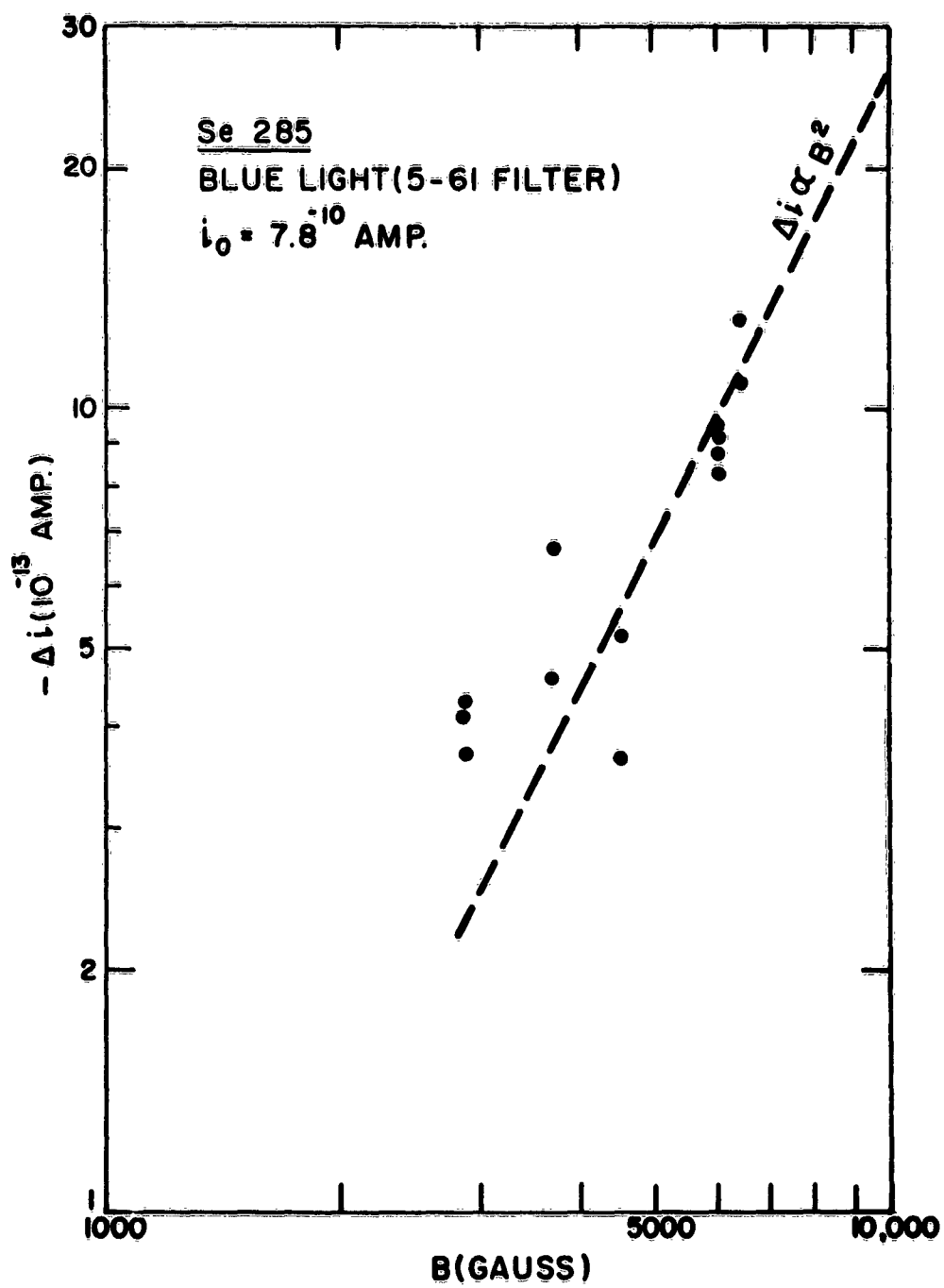
FIG. II-3

from which the average magnetoresistance of the sample can be obtained. The scatter of points is too great to determine whether the $\Delta i \propto B^2$ law, characteristic of classical magnetoresistance is applicable. However, the magnitude of the effect to be expected can be calculated from

$$\frac{\sigma}{\sigma_{B=0}} = 1 - \mu^2 B^2 \left(\frac{8}{\pi} - 2\right)$$

For $\mu = 0.1$ cm^{2}v^{-1}s^{-1}, the predicted value of $\Delta\sigma/\sigma_{B=0} \approx 10^{-11}$ at 6000 gauss while Fig. II-3 shows $\Delta\sigma/\sigma_{B=0} \approx 10^{-3}$. In this case it is clear therefore that the magnetoresistance is the result of the inhomogeneous conductivity introduced by heat treatment of the sample, as discussed above.

11

III. "TIME-OF-FLIGHT" MEASUREMENTS WITH TRANSIENT UNIPOLAR SPACE CHARGE LIMITED CURRENTS

1. INTRODUCTION

It has recently been demonstrated that ohmic contact formation is possible to a variety of insulators, both inorganic (CdS[24], ZnS[25], Se[16], I_2[26]) and organic (anthracene[6], p-terphenyl[3], p-quaterphenyl[3], phthalocyanine[13]), either by a suitable choice of electrodes or by photogeneration of free carriers near the surface of the crystal with strongly absorbed light. With such contacts, space-charge-limited current flow may readily be observed.[3,6,13,16,24-26] When no carrier trapping occurs, the steady state current density j_{ss} obeys Child's Law for solids[27] which has the following form in mks units for a plane-parallel electrode geometry:

$$j_{ss} = \frac{9}{8} \epsilon \mu \frac{V^2}{d^3} . \tag{1}$$

Here, j is the current density, ϵ is the electric permittivity, μ is the carrier mobility, V is the applied voltage and d is the interelectrode spacing. In principle, this relation can be used to obtain μ from steady state current voltage measurements. In fact, however, carrier trapping either reduces the current density by orders of magnitude[28] or alters the current voltage dependence entirely[3,28]. For this reason, it becomes necessary to observe essentially trap-free carrier transport with transient current measurements. The basic idea is that even when trapping occurs, it takes some time to fill the traps with the injected carriers so that immediately after injection, essentially trap-free current flow may be approached. This technique has been successfully applied by Smith and Rose[24] to CdS and by Mark and Helfrich to p-terphenyl[3]. Even more important is the realization that the injected carrier front moves through the crystal with a finite velocity which makes it possible to measure the transit time of this carrier front by a "time-of-flight" measurement.

2. THEORY OF "TIME-OF-FLIGHT" MEASUREMENT

The space-charge-limited "time-of-flight" measurement was first reported by Many and co-workers[26] and by Helfrich and Mark[6], and was later treated in great detail by Many and Rakavy[7]. The salient features of the "time-of-flight" measurement, for the trap free case, are illustrated by the solid curve of Fig. III-1. At $t=0$ (it is assumed that the applied
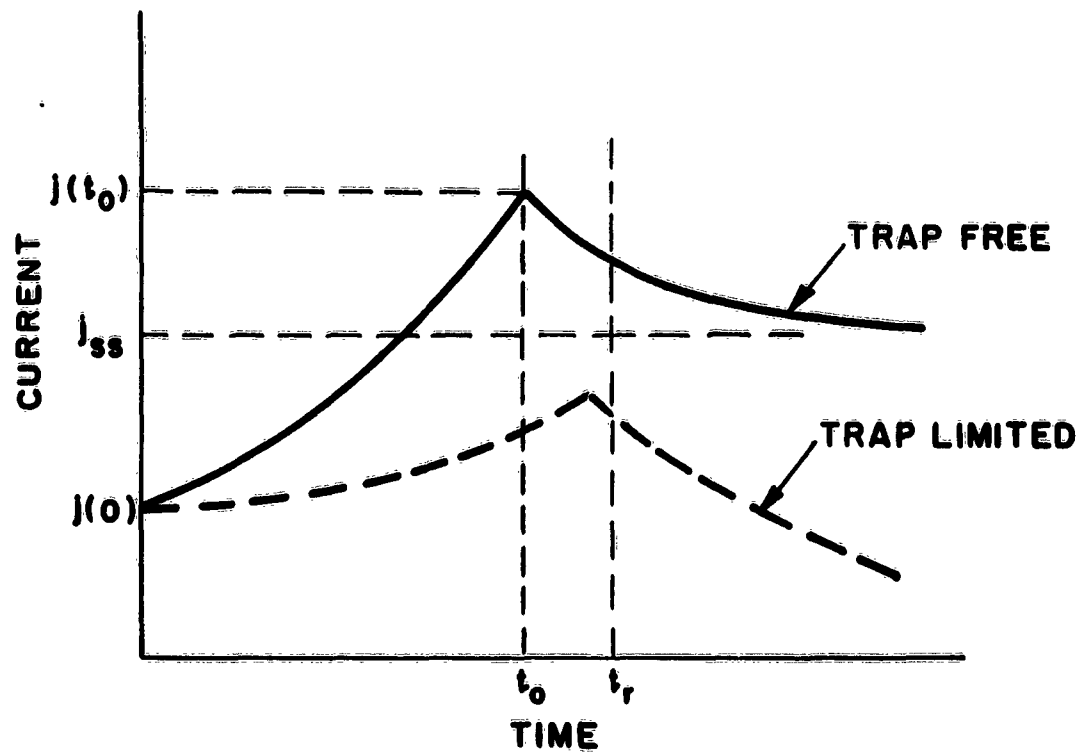
$$j(0) = 0.445\, j_{ss}, \quad j(t_0) = 1.2\, j_{ss}, \quad t_0 = 0.786\, t_r$$

$$t_r = d^2/\mu V, \quad j_{ss} = (9/8)\xi\mu(V^2/d^3)$$

FIG. III-1   TRANSIENT UNIPOLAR SPACE CHARGE LIMITED CURRENT

13

voltage rises instantaneously to its steady-state value), the injected space charge resides on the surface of the crystal viewed as a capacitor. As t increases, the crystal begins to fill with space charge, located behind a well defined carrier front which advances through the crystal from the injecting electrode with a time dependent velocity proportional to the field at the carrier front. As the front advances, the crystal fills with space charge and its capacitance increases with time. The total current also increases with time until the carrier front arrives at the exit electrode (which may be either ohmic or blocking) after the time $t_o = 0.786\ t_r$ where t_r is the uniform field (space charge free) transit time $d^2/\mu V$. The "time-of-flight" t_o of the carrier front is less than t_r because the field at the carrier front is always greater than the uniform field V/d. A cusp appears in the current at t_o because the center of the space charge distribution lies closer to the exit electrode at t_o than in the steady state. As t increases beyond t_o, the redistribution of the injected space charge causes the current to decay from the cusp to the lower steady state value given by Eq. (1). The lower dashed curve of Fig. III-1 represents the transient under conditions of weak trapping[7] (mean free trapping time long compared with t_r). It lies beneath the trap free curve, peaks at a time between t_o and t_r, but has the same value at $t = 0$, and decays to a lower steady state current the magnitude of which is determined by the traps[28]. This decay may serve as a valuable tool for studying trapping.

The analytic form of the trap free transient is given[6,7,26] by

$$j(t) = 0.455\ j_{ss}\ \left[1 - \frac{t}{2t_r}\right]^{-2}\ ;\ 0 \leq t \leq t_o \tag{2}$$

$$j(t) = 1.23\ j_{ss}\ \frac{(t_o/t_r)^2}{\left[1 - 0.65\ \ell n\frac{t}{t_o}\right]^2}\ ;\ t_o \leq t \leq 1.51\ t_o \tag{3}$$

$$j(t) = j_{ss} = \frac{9}{8}\ \epsilon\mu\ \frac{V^2}{d^3}\ ;\ t \geq 1.51\ t_o\ . \tag{4}$$

These equations are obtained from the current density and Poisson's equation with the boundary condition zero field at the injecting electrode which is the analytical definition of an ohmic contact. Equation (2) describes the rise of the transient in the "time-of-flight" interval up to the appearance of the cusp and Eq. (3) describes the decay of the current to the steady state. The entire transient varies as V^2/d^3 and the time of flight t_o is proportional to $1/V$ when the mobility is field independent. The mobility can therefore be obtained in two independent ways; from the magnitude of the current transient and from measurement of t_o. As mentioned, weak trapping changes the shape of the transient somewhat[7]. The time of

14

flight t_o increases slightly, but never exceeds t_r (the field at the carrier front is never less than V/d) and the cusp is reduced in magnitude. The initial value of the current at $t = 0$ is, however, not affected by trapping. Hence, weak trapping does not alter the picture significantly. It introduces a small uncertainty in t_o but does not change the value of the current at $t = 0$.

There are three important characteristics of the transient: the magnitude of the initial current $j(0)$ which is not affected by trapping, the magnitude of the cusp $j(t_o)$ which is affected by trapping, and the time of flight t_o which is also affected by trapping. The ratio $j(t_o)/j(0)$ can be used as a criterion for trapping. From Eq. (2), the ratio is 2.7 for the trap free case. It will be smaller when trapping takes place, and therefore serves to indicate that t_o lies not at $0.786\ t_r$ but somewhere in the interval $0.786\ t_r < t_o \le t_r$. These considerations are an idealization of what occurs in practice for it has been assumed in the derivation of Eqs. (2) and (3) that the measuring circuit has zero time constant. It is therefore important to ascertain the effect of a finite circuit time constant on the experimental determination of the parameters $j(0)$, $j(t_o)$ and t_o.

3. EFFECT OF A FINITE CIRCUIT TIME CONSTANT ON THE "TIME-OF-FLIGHT" MEASUREMENT

A finite time constant will introduce two adverse effects[29]. It will give rise to a capacitive voltage across the load resistor which may be orders of magnitude larger than the signal voltage at very short times and thus may mask the latter entirely. In addition, a finite time constant may also distort the shape of the ideal transient and thereby reduce the amount of information which may be extracted from the measurement. The first of these difficulties is severe only when the carriers are injected through a steady state ohmic contact by a voltage pulse. It presents no problems when a photogenerated ohmic contact is used because here a steady voltage is applied to the sample and the transient is produced by flashing the light. The capacitive spike can be reduced by using a balanced circuit[6]. A voltage divider with the center terminal grounded is connected across the voltage source which is now floating. The crystal is connected to one pole and a variable capacitor to the other, and the two signals are added algebraically in front of the load resistor. The variable capacitor is then adjusted so as to cancel the capacitive transient at the load resistor. Distortion of the transient by a finite circuit time constant is always present however, regardless of the way in which the carriers are injected. Denoting the circuit time constant by τ, the current through the load resistor is given by[29]

$$\frac{j(t)}{i_{ss}} = \frac{a}{x} - a\,e^{-a(1-x)} + a^2\,e^{ax}\int_1^x \frac{e^{-ax}}{x}\,dx \qquad (5)$$

15

where

$$a = 2t_r / \tau \tag{6}$$

and

$$x = 1 - (t/2t_r). \tag{7}$$

The parameter a, which contains τ, is a measure of the departure from the ideal case $\tau = 0$. For large a, Eq. (5) becomes

$$\frac{j(t)}{j_{ss}} = \left[1 - \frac{t}{2t_r} \right]^{-2} - \exp \left[\frac{-at}{2t_r} \right] \tag{8}$$

which differs from Eq. (2) by the exponential term on the right. The distortions produced by a finite τ are best illustrated by Fig. III-2 which is a plot of Eq. (5) for various values of a. When a becomes less than 100, extrapolation to $j(0)$ begins to fail. For $a < 50$, the cusp begins to decrease in magnitude and for $a < 10$, the shape of the transient becomes so badly distorted that the cusp becomes indistinguishable. To observe undistorted transients (i.e., true values of $j(0)$, $j(t_o)$ and t_o), a should be kept greater than 100.

The limitations imposed by the measuring circuit define a finite band of applied voltages over which significant time-of-flight measurements can be made. The high voltage end V_t of this band is essentially set by the response time of the circuit and is given by

$$V_t = \frac{2d^2}{\mu a_o RC} \; ; \; RC = \tau \tag{9}$$

where R is the load resistance and C is the total circuit capacitance. Since a is proportional to t, and hence inversely proportional to V, its value is not constant over the whole voltage band. In Eq. (9) the *numerical value* a_o given to a is its value at V_t. Then a increases as V is reduced below V_t and the transients at lower voltages will conform more closely to the true transients. The lower end V_i of the band is set by the sensitivity of the circuit and is given by

$$V_i = \left[\frac{9}{8\epsilon a} \cdot \frac{d^3}{\mu} \cdot \frac{V_s}{R} \right]^{\frac{1}{2}} \tag{10}$$

where a is the electrode area and V_s is the voltage detectability of the amplifier. The logarithmic width ΔV of the band is defined by the ratio V_t/V_i and is given by

$$\Delta V \equiv \frac{V_t}{V_i} = \left[\frac{32\epsilon a}{9} \cdot \frac{d}{\mu} \right]^{\frac{1}{2}} \cdot \left[\frac{1}{a_o C (R V_s)^{\frac{1}{2}}} \right]. \tag{11}$$

16
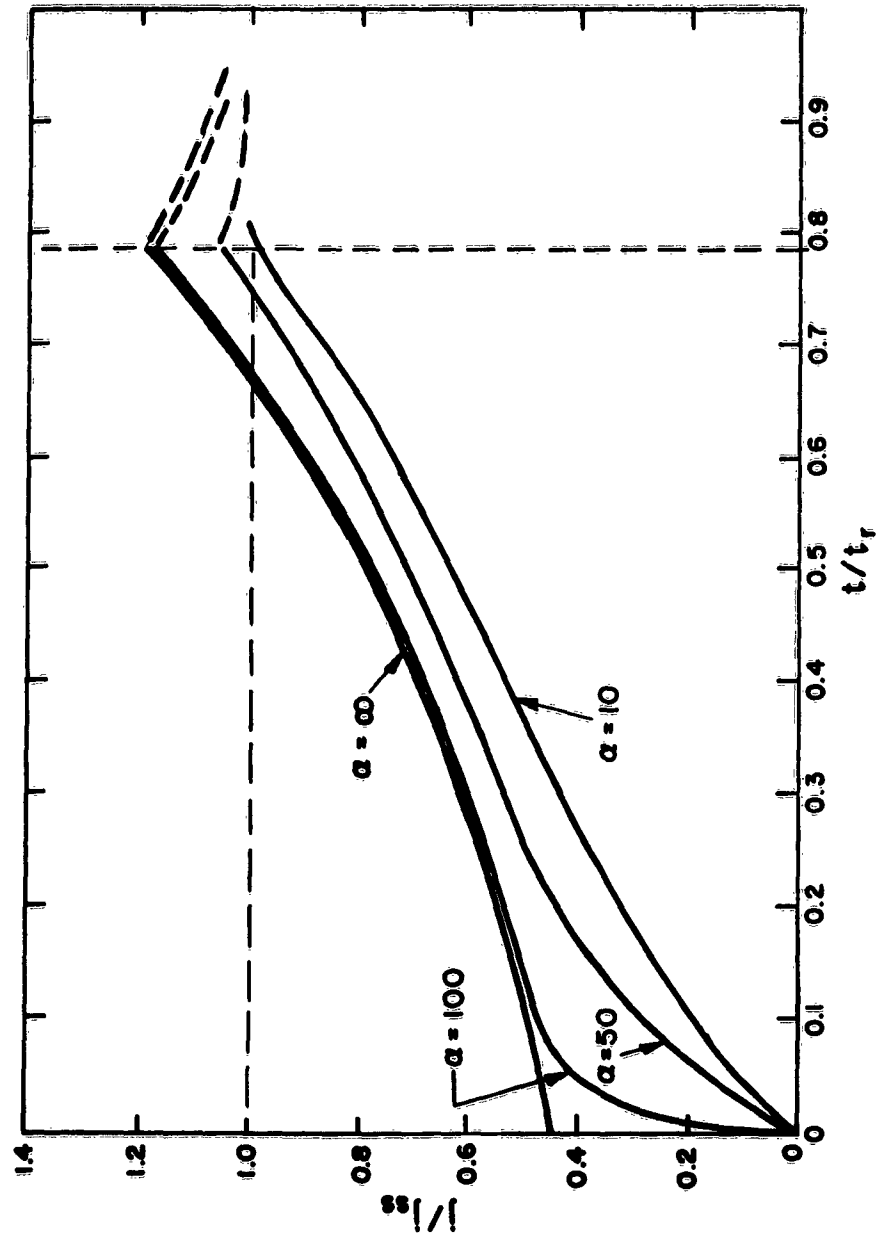
FIG. III-2   TRANSIENT SPACE CHARGE LIMITED CURRENT FOR FINITE
CIRCUIT TIME CONSTANT

17

As might be expected, Eq. (11) shows that ΔV becomes wider the more sensitive and the faster the circuit. In addition, for a given gain-bandwidth product of the circuit ΔV is also widened and shifted to higher voltages when the crystal is made thicker. In order to observe the transient at all, $\Delta V > 1$. This condition puts a lower limit on the thickness of the crystal, given by

$$d = \left[\frac{9(a_o C)^2 RV_s}{32 Ga} \right] \mu \qquad (12)$$

and shows that the higher the mobility of the material, the thicker must be the crystal being examined in order to study transport by this time-of-flight method. There is, however, an upper limit to the crystal thickness which is set by trapping. If the crystal is so thick that a large fraction of the injected carriers are trapped before they reach the exit electrode, no distinctive transient is observed.

These considerations are summarized by Fig. III-3 which is a plot on a logarithmic field of the current $i(0) \equiv j(0) \cdot a$ and t_r as a function of the voltage for an arbitrary set of parameters. The circuit limitations τ and $i_s = V_s/R$ are shown on the appropriate axes. The voltage band ΔV is represented by the heavy line labelled "ΔV". Increasing the thickness of the crystal will lower the current curve more than it will raise the transit time curve. Because of this and the different slopes of the two curves ($i(0) \sim V^2$ and $t_r \sim V^{-1}$) it is clear that increasing d widens ΔV and shifts it to higher voltages. The influence of carrier trapping has also been included in this figure. The current transient can only appear when t_r is comparable or less than t_f, the mean free time of the injected carriers before capture by deep traps. Let the ratio $(t_r/t_f \equiv \beta)$. Then the above condition requires that $\beta < 1$. When the transit time exceeds βt_f, the time-of-flight transient cannot be observed which is the same as saying that no measurement can then be made at voltages less than $V_f = d^2/\mu\beta t_f$. In the figure, βt_r has been chosen so that $V_f > V_i$ to illustrate how trapping can narrow the voltage band. This trap limited voltage band is labelled "ΔV_f" in the figure. A plot of this kind for a given material under investigation serves as a very good order of magnitude guide for an experimenter who wishes to observe these time-of-flight pulses.

4. DISCUSSION

The time-of-flight measurements need not be carried out under space charge limitation[8]. If this restriction is removed, the transit time of a carrier pulse may still be observed. However, there are two advantages of working under space charge limitation.

18
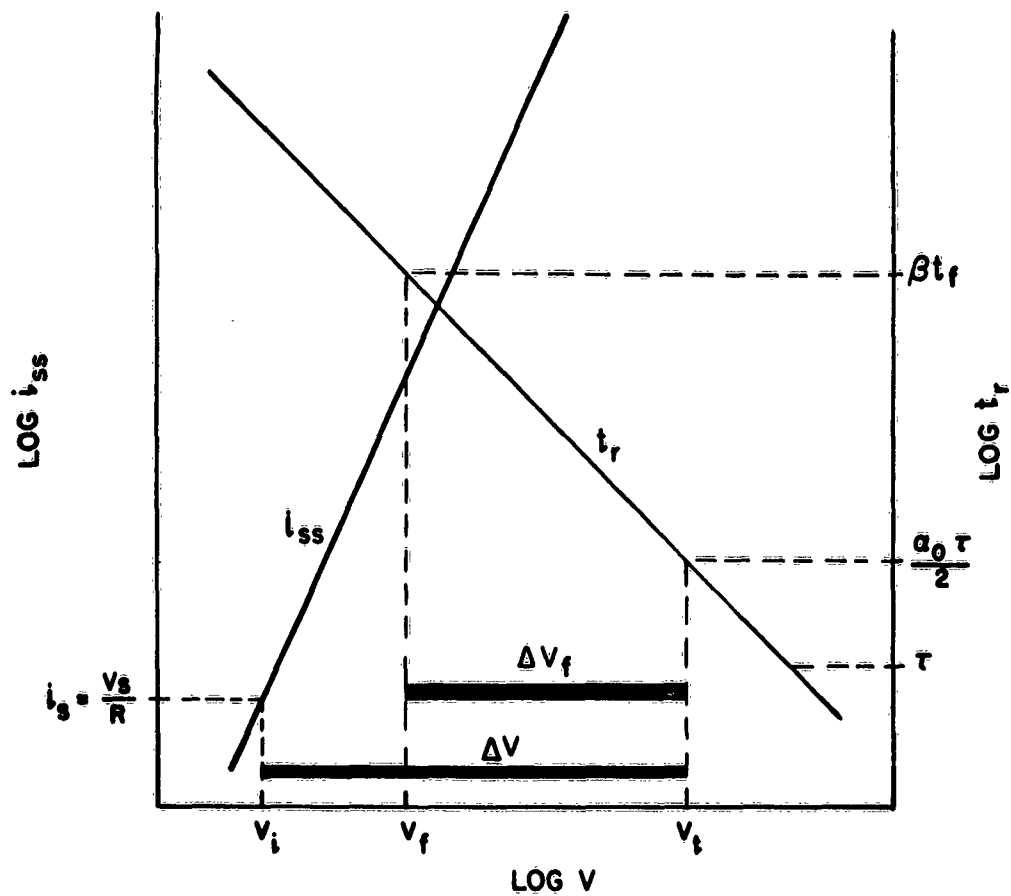
FIG. III-3 ILLUSTRATION OF VOLTAGE BANDS FOR OBSERVING TRANSIENT SPACE CHARGE LIMITED CURRENTS

The first is that diffusion effects are not as severe. If a pulse of carriers drifts through
the crystal, it will spread out as it moves and may be sufficiently broad by the time it
reaches the exit electrode so as to introduce a considerable uncertainty in the measurement
of the transit time. Under space charge limitation, it is not a pulse of carriers which moves
through the crystal but rather a cloud of carriers which always fills the entire space between
its front and the injecting electrode. Hence diffusion of carriers will not be as important.
The second advantage of measuring under space charge limitation is that each measurement
is in reality two independent measurements: one of the magnitude of the current and the
other of the time-of-flight of the carrier front. Both measurements yield the mobility and may
be used to check each other, so to speak. The space charge limited method also shows very
characteristic effects of trapping which makes it possible to use the method to study certain
trapping effects.

We propose to apply this technique to the study of carrier transport in insulators
in order to supplement the Hall effect measurements.

IV. A GENERAL ANALYSIS OF UNIPOLAR STEADY STATE SPACE CHARGE LIMITED CURRENTS IN INSULATORS WITH VARIOUS ELECTRODE GEOMETRIES AND TRAP DISTRIBUTIONS

1. INTRODUCTION

Unipolar space charge limited current flow in solids has been observed in many materials and analysed theoretically under trap free conditions as well as for various distributions[5]. To date, both the experimental and the theoretical studies have dealt exclusively with a plane-parallel electrode geometry. Recently, Many[30] has presented a trap free analysis for two non-planar electrode configurations: the cylindrical geometry in which the insulator fills the space between two coaxial cylindrical electrodes and the hemispherical geometry, which is a good approximation to a point-contact configuration, where the medium fills the space between two hemispherical cap electrodes. The main conclusion of Many's analysis[30], insofar as space charge limited current flow is concerned, is that a non-planar electrode configuration causes rectification on purely geometric grounds. That is, both electrodes can be physically the same and indeed must form ohmic contact[24] to the insulator in order for space charge limited currents to flow.

In most real materials, trap free space charge limited currents can only be observed under transient conditions[3,6,24,26]. In the steady state, trapping of the injected carriers very often considerably alters the space charge limited current-voltage relations[28]. It is therefore of some practical value to examine the influence of trapping on space charge limited currents flow in insulators with non-planar electrode configurations. We do so here by adopting a very general approach to the analysis which encompasses collectively the following cases: trap free, single shallow trap level and exponential trap distribution each for the plane-parallel, cylindrical and hemispherical (point-contact) electrode configurations. The basic equations for unipolar space charge limited current flow are written in terms of a generalized interelectrode coordinate normal to the electrode surfaces which are always considered parallel and the relation between the free and trapped injected excess carrier concentrations is left unspecified. A general first order differential equation for the field is derived from which the trap free as well as the two trap limited cases can be obtained for all three electrode geometries collectively by choosing the proper analytic dependence between the free and trapped charge. The three resulting differential equations

21

for the field are then integrated twice to give three general current-voltage relations each of which contains two parameters a systematic choice for which leads, in turn, to the specific current-voltage equations for each of the electrode configurations under consideration. Thus, we derive most generally the already familiar trap free and trap limited space charge limited current relations for the plane-parallel geometry[3,28] as well as Many's space charge limited current equations and rectification ratios for the trap free non-planar configurations[30]. In addition, we also obtain the trap limited space charge limited current relations and rectification ratios for the non-planar geometries.

We shall show quite generally, as Many has done for the trap free cases, that rectification is a direct consequence of a non-planar electrode configuration and that the magnitude of the rectification ratios can be profoundly influenced by the nature of the trap distribution. In particular, shallow discrete traps do not alter the rectification ratios predicted by Many in his trap free analysis[30] but an exponential trap distributions can, in principle, substantially increase the rectification ratios. We shall neglect diffusion effects in the analysis and shall write the equations in mks units.

2. BASIC EQUATIONS

We consider a generalized one dimensional geometry in which the electrodes are parallel but not necessarily planar. An interelectrode distance coordinate p is defined which is oriented normal to the electrode surfaces. One electrode is situated at p_1 and the other at p_2. In the non-planar cases, p_1 and p_2 are radii and we shall always consider $p_2 > p_1$. For the plane-parallel geometry the electrode area is A and for the cylindrical geometry the length of the cylinder is L. Edge effects will be neglected. For definiteness, we choose electrons as the carriers injected by the ohmic contact.

The analysis involves the simultaneous solution of the following set of equations:

$$j(p) = e\mu n_s(p) \mathcal{E}(p) \tag{1}$$

$$j(p) = i/\gamma p^\alpha \tag{2}$$

$$\nabla \cdot \mathcal{E}(p) = \frac{e}{\epsilon} n_T(p) \tag{3}$$

$$n_f(p) + n_t(p) = n_T(p) \tag{4}$$

$$n_t(p) = f[n_f(p)]. \tag{5}$$

In these equations:

p = generalized interelectrode coordinate

γ = $\begin{cases} A & \text{for the plane-parallel case} \\ 2\pi L & \text{for the cylindrical case} \\ 2\pi & \text{for the hemispherical case} \end{cases}$

a = $\begin{cases} 0 & \text{for the plane-parallel case} \\ 1 & \text{for the cylindrical case} \\ 2 & \text{for the hemispherical case} \end{cases}$

$j(p)$ = current density

i = measured current

e = elementary charge 1.6×10^{-19} coulombs

ϵ = electric permittivity (dielectric constant) $\times$ (8.8×10^{-12} f/m)

μ = microscopic scalar mobility assumed field independent

$\mathcal{E}(p)$ = electric field

$n_T(p)$ = total excess injected carrier concentration

$n_f(p)$ = concentration of carriers in conducting states

$n_t(p)$ = concentration of carriers in the traps.

Equation (1) is the diffusion free current density, Eq. (2) is the general relation between the total current and the position dependent current density, Eq. (3) is Poisson's Equation which must be satisfied since charge neutrality is violated, Eq. (4) is a conservation equation which states that when traps are present the injected carriers are distributed among conducting and trapping states and Eq. (5) is the general representation of the functional dependence between the free and trapped carriers and is also only valid when trapping occurs. A particular choice of a trapping model will give us an analytical representation of Eq. (5). Usually, the assumption $n_f \ll n_t$ is also made to simplify the calculation[3,28]. This means that we may write

$$n_t(p) \cong n_T(p) \tag{4a}$$

instead of Eq. (4) so that Eq. (5) becomes a relation between n_f and n_T:

$$n_T(p) = f[n_f(p)]. \tag{5a}$$

We shall follow this procedure. When no trapping takes place, Eqs. (4a) and (5a) must be replaced by the identity

$$n_f(p) \equiv n_T(p). \tag{6}$$

Mathematically, the trap free case follows when the function f of Eq. (5a) is replaced by the operator dimensionless unity.

The basic equations are solved with the boundary condition zero field at the injecting electrode which is the mathematical definition of an ohmic contact[28]. This condition can be most generally written as

$$\mathcal{E}(p_{1,2}) = 0 \tag{7}$$

by which we mean the following. When electrode p_1 is injecting the excess carriers, $p_{1,2} \equiv p_1$ and we shall label the resultant space charge limited currents i_1. By the same token, when electrode p_2 is the source of the injected carriers, $p_{1,2} \equiv p_2$ and the resultant currents are denoted by i_2. We call i_1 and i_2 currents because each symbol actually represents nine currents: the trap free and the two trap limited currents each for the three electrode configurations.

3. OUTLINE OF THE GENERAL SOLUTION

The basic equations (1), (2), (3), (4a) and (5a) can be combined to give the following general equation for the field (p):

$$\frac{d\mathcal{E}(p)}{dp} + \frac{a}{p} \, \mathcal{E}(p) = \frac{e}{\epsilon} \, f\left[\frac{i}{\gamma\mu\epsilon p^a \, \mathcal{E}(p)}\right]. \tag{8}$$

The next step in the solution is to assign an analytic representation to the function f through which process the details of trapping are introduced into the problem. We then have three differential equations, one each for the trap free and the two trap limited cases. These three equations are then solved with the help of the generalized boundary condition (7) for the generalized field $\mathcal{E}(p)$. Next, the three field equations are integrated over the inter-electrode coordinate p to give three equations for the potential V and these equations are then solved for the currents $i_{1,2}$ which gives us three generalized space charge limited current-voltage equations. From each of these equations, we obtain three current relations, one for each electrode configuration, by setting $a = 0$, 1 or 2 for the plane-parallel, cylindrical and hemispherical geometries respectively and by assigning the proper value to γ. Finally, each of *these* three current equations represents two relations: i_1 for p_1 injecting and i_2 for p_2 injecting. We therefore obtain 18 current equations from Eq. (8). For the planar geometry, i_1 and i_2 are degenerate as might be expected from symmetry conditions. For the non-planar geometries, i_1 and i_2 differ by voltage independent factors which are just the rectification ratios. This procedure is quite general and is valid, in principle, for any electrode configuration and trap distribution.

4. TRAP FREE CASE

According to Eq. (6), we must replace I in Eq. (8) by the operator dimensionless unity. Hence we have

$$\frac{d\mathcal{E}}{dp} + \frac{a}{p}\mathcal{E} = \frac{i}{\gamma\mu\epsilon p^a \mathcal{E}}. \qquad (9)$$

The field $\mathcal{E}(p)$ can be eliminated from the right side of this equation by multiplying both sides by $2\mathcal{E}(p)$. We also define the new variable $F(p)$ according to

$$F(p) = [\mathcal{E}(p)]^2. \qquad (10)$$

We then obtain the simple differential equation

$$\frac{dF}{dp} + \frac{2a}{p}F = \frac{2i}{\gamma\mu\epsilon p^a} \qquad (11)$$

which is immediately solvable by the integrating factor method to give the general solution

$$F(p) = \frac{2i}{\gamma\mu\epsilon(1+a)} p^{1-a} \left[1 + \frac{C\gamma\mu\epsilon(1+a)}{2i}\left(\frac{1}{p}\right)^{1+a}\right] \qquad (12)$$

where C is a constant. Using the boundary condition (7) to evaluate C and Eq. (10) to obtain the field, Eq. (12) becomes

$$\mathcal{E}(p) = \left[\frac{2i}{\gamma\mu\epsilon(1+a)}\right]^{1/2} \left\{p^{1-a}\left[1 - \left(\frac{p_{1,2}}{p}\right)^{1+a}\right]\right\}^{1/2}. \qquad (13)$$

The potential is found by integrating Eq. (13) over the interelectrode coordinate p. Hence

$$V = \int_{\Delta p_{1,2}} \mathcal{E}(p)\,dp = \left[\frac{2i}{\gamma\mu\epsilon(1+a)}\right]^{1/2} I_{1,2}(p_1, p_2) \qquad (14)$$

where

$$I_{1,2}(p_1, p_2) = \int_{\Delta p_{1,2}} \left\{p^{1-a}\left[1 - \left(\frac{p_{1,2}}{p}\right)^{1+a}\right]\right\}^{1/2} dp. \qquad (15)$$

The integral (15) is to be interpreted as follows. For the generalized currents i_1, $I_{1,2} = I_1$, $p_{1,2} = p_1$ and $\Delta p_{1,2}$ signifies integration from p_1 to p_2 whereas for the generalized currents i_2, $I_{1,2} = I_2$, $p_{1,2} = p_2$ and the integration runs from p_2 to p_1. From Eq. (14) we obtain the generalized space charge limited currents $i_{1,2}$ for the trap free case:

$$i_{1,2} = \frac{\epsilon\mu\gamma(1+a)}{2}\frac{V^2}{[I_{1,2}(p_1, p_2)]^2}. \qquad (16)$$

25

A. PLANAR CONFIGURATION

Here $a = 0$ and $\gamma = A$. From Eq. (15) we have that

$$I_{1,2}(p_1, p_2) = \int_{p_2}^{p_2} (p - p_{1,2})^{1/2} \, dp = \frac{2}{3} (p_2 - p_1)^{3/2} \tag{17}$$

where $(p_2 - p_1)$ is just the interelectrode spacing, and from Eq. (16)

$$i_{1,2} = \frac{9}{8} \epsilon\mu \frac{V^2}{(p_2 - p_1)^3} \tag{18}$$

which is just the familiar space charge limited current formula first derived by Mott and Gurney[27]. The currents $i_{1,2}$ are degenerate; that is $i_1 \equiv i_2$ as we had expected.

B. CYLINDRICAL CONFIGURATION

For this case $a = 1$ and $\gamma = 2\pi L$. Equation (15) now reads

$$I_{1,2}(p_1, p_2) = \int_{\Delta p_{1,2}} \left[1 - \left(\frac{p_{1,2}}{p} \right)^2 \right]^{1/2} \, dp. \tag{19}$$

For the moment, we shall consider $p_2 p_1$ under which condition

$$I_1 \xrightarrow[p_2 \gg p_1]{} \int_{p_1}^{p_2} dp \xrightarrow[p_2 \gg p_1]{} p_2 \tag{20a}$$

and

$$I_2 \xrightarrow[p_2 \gg p_1]{} \int_{p_1}^{p_2} \frac{p_2}{p} \, dp = p_2 \, \ell n\left(\frac{p_2}{p_1} \right) . \tag{20b}$$

Hence

$$i_1 = 2\pi\epsilon\mu L \frac{V^2}{p_2^2} \tag{21a}$$

and

$$i_2 = 2\pi\epsilon\mu L \frac{V^2}{p_2^2} \left[\ell n \frac{p_2}{p_1} \right]^{-2} \tag{21b}$$

which is Many's equation for the cylindrical case[30]. The currents i_1 and i_2 are not the same. The former is always greater than the latter and the rectification ratio ρ is given by

$$\rho = \frac{i_1}{i_2} = \left[\ell n \frac{p_2}{p_1} \right]^2. \tag{22}$$

C. HEMISPHERICAL CONFIGURATION

Now $a = 2$ and $\gamma = 2\pi$. The integral (15) is

$$I_{1,2} = \int_{\Delta p_{1,2}} \left\{ \frac{1}{p} \left[1 - \left(\frac{p_{1,2}}{p} \right)^3 \right] \right\}^{\frac{1}{2}} dp \tag{23}$$

Again for $p_2 \gg p_1$,

$$I_1 \xrightarrow[p_2 \gg p_1]{} \int_{p_1}^{p_2} p^{-\frac{1}{2}} \, dp \xrightarrow[p_2 \gg p_1]{} 2p_2^{\frac{1}{2}} \tag{24a}$$

and

$$I_2 \xrightarrow[p_2 \gg p_1]{} \int_{p_1}^{p_2} \left[\frac{1}{p} \left(\frac{p_2}{p} \right)^3 \right]^{\frac{1}{2}} dp = p_2^{\frac{1}{2}} \left(\frac{p_2}{p_1} \right). \tag{24b}$$

The respective currents are

$$i_1 = \frac{3\pi}{4} \epsilon\mu \, \frac{v^2}{p_2} \tag{25a}$$

and

$$i_2 = \frac{3\pi}{4} \epsilon\mu \, \frac{v^2}{p_2} \left(\frac{p_2}{2p_1} \right)^{-2} \tag{25b}$$

and the rectification ratio is

$$\rho = \left(\frac{p_2}{2p_1} \right)^2 \tag{26}$$

which, as Many has pointed out[30], can be very large.

27

5. SINGLE SHALLOW TRAP LEVEL

This is the case first treated by Rose[20,28] for the planar electrode configuration. By a shallow trap, we mean that the position dependent quasi Fermi level $\bar{E}_f(p)$ lies sufficiently below the trap level so that Bolzmann statistics apply. The assumed energy level scheme is illustrated on Fig. IV-1. Under these assumptions, the free carrier concentration is

$$n_f(p) = N_o \ \exp - \left[\frac{E_c - E_f(p)}{kT} \right] \tag{27}$$

and the trapped carrier concentration, which is here set approximately equal to the total excess carrier concentration, is

$$n_T(p) = N_t \ \exp - \left[\frac{\bar{E}_t - \bar{E}_f(p)}{kT} \right] . \tag{28}$$

Here N_o is the effective density of states in the conduction band, N_t is the concentration of traps located at an energy $\bar{E}_t$ and $\bar{E}_c$ is the energy of the bottom edge of the conduction band. From Eqs. (27) and (28), we obtain the ratio

$$\frac{n_f}{n_-} = \frac{N_o}{N_t} \ \exp - \left[\frac{E_c - \bar{E}_t}{kT} \right] = \theta(T) \tag{29}$$

the well known θ-factor of Rose[20,28]. Hence f in Eq. (8) must be replaced by the multiplicative operator $1/\theta$ which is, of course, a constant factor at a given temperature. The analysis of the shallow trap case is therefore the same as that of the trap free case except that the factor $1/\theta$ must be included linearly on the right side of Eq. (16) The θ-factor merely reduces the magnitude of all the currents by the same amount without altering their dependence on any of the parameters in the trap free analysis. Hence the rectification ratios for the shallow trap case are the same as those of the trap free case.

6. EXPONENTIAL TRAP DISTRIBUTION

By an exponential trap distribution we mean that the volume concentration of the trapping states per unit interval of energy $\eta_t(E)$ can be approximated by the distribution[3,20,28]

$$\eta_t(E) = \frac{N_t}{kT_c} \ \exp - \left(\frac{\Delta E}{kT_c} \right) \tag{30}$$

28

CONDUCTION BAND

//////////////////////////////////// E_c

N_t — — — — — — — — — — — E_t

— — — — — — — — — — — E_f

/////////////////////////////

VALENCE BAND
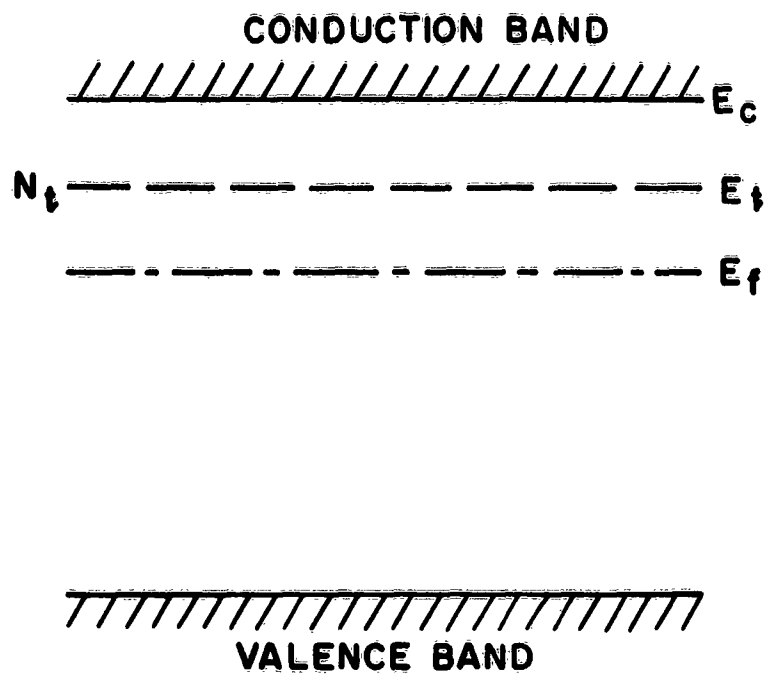
FIG. IV-1   ENERGY BAND SCHEME FOR
SINGLE SHALLOW TRAPPING
LEVEL

where $\Delta E = E_c - E > 0$ and kT_c is an energy constant characteristic of the distribution which describes the steepness of the function (30). To a good approximation at room temperature, n_t is obtained by integrating the distribution (30) from some low lying energy, which for analytical purposes is set at $-\infty$ [28], up to the quasi Fermi level $E_f(p)$. Thus, in terms of our notation, n_T $(\simeq n_t)$ is given by

$$n_T(p) = -\int_{-\infty}^{\Delta E_f(p)} \eta_t(\Delta E)\, d(\Delta E) = N_t \exp - \left[\frac{\Delta E_f(p)}{kT_c}\right] \tag{31}$$

where $\Delta E_f(p) = E_c - E_f(p)$ and where it must be remembered that $E_f(p)$ is a function of p because the space charge is not in general homogeneously distributed throughout the volume of the insulator. The minus sign occurs in front of the integral because of our notation, ΔE decreases over the interval of integration. So long as $\Delta E_f(p)$ remains larger than about $5kT$, we may use Eq. (27) to obtain the free carrier concentration. We now have a parametric representation for Eq. (5), the parameter being E_f. Equations (27) and (31) may now be solved for an explicit relation between n_T and n_f by eliminating the parameter E_f. Thus we have

$$n_T = N_t \left(\frac{n_f}{N_o}\right)^{1/\ell} \tag{32}$$

where we have set

$$\ell \equiv T_c/T \tag{33}$$

a quantity which must always be greater than unity for the analysis to have physical significance [28]. Equation (32) is an analytical representation of Eq. (5a). The function f in Eq. (8) may now be replaced by the operator

$$f = N_t N_o^{1/\ell} [\quad]^{1/\ell}$$

so that Eq. (8) now reads

$$\frac{d\mathcal{E}(p)}{dp} + \frac{a}{p}\,\mathcal{E}(p) = \frac{e}{\epsilon}\,N_t \left[\frac{i}{\gamma N_o \mu e p^a \mathcal{E}(p)}\right]^{1/\ell}. \tag{34}$$

The solution of this equation is very similar to that of Eq. (9). The field $\mathcal{E}(p)$ is eliminated from the right side of Eq. (34) by multiplying through by $[(\ell + 1)/\ell][\mathcal{E}(p)]^{1/\ell}$ and the equation is simplified by defining the new variable

$$\bar{F}(p) = [\mathcal{E}(p)]^{\frac{\ell+1}{\ell}} \tag{35}$$

which process leads to the equation

$$\frac{d\bar{F}}{dp} + \frac{a}{p}\left(\frac{\ell+1}{\ell}\right) F = \left(\frac{\ell+1}{\ell}\right)\frac{eN_t}{\epsilon}\left[\frac{i}{\gamma N_t e \mu p^a}\right]^{1/\ell}. \tag{36}$$

In strict analogy to the procedure followed in the trap free analysis, the solution of Eq. (34) can be written down at once

$$\mathcal{E}(p) = \left[\frac{eN_t(\ell+1)}{\epsilon\ell(1+a)}\right]^{\frac{\ell}{\ell+1}}\left[\frac{i}{\gamma N_o e\mu}\right]^{\frac{1}{\ell+1}} p^{\frac{\ell-a}{\ell+1}}\left[1-\left(\frac{p_{1,2}}{p}\right)^{1+a}\right]^{\frac{\ell}{\ell+1}}. \tag{37}$$

The potential is

$$V = \int_{\Delta p_{1,2}}\mathcal{E}(p)\,dp = \left[\frac{eN_t(\ell+1)}{\epsilon\ell(1+a)}\right]^{\frac{\ell}{\ell+1}}\left[\frac{i}{\gamma N_o e\mu}\right]^{\frac{1}{\ell+1}} J_{1,2}(p_1, p_2) \tag{38}$$

where

$$J_{1,2}(p_1, p_2) = \int_{\Delta p_{1,2}} p^{\frac{\ell-a}{\ell+1}}\left[1-\left(\frac{p_{1,2}}{p}\right)^{1+a}\right]^{\frac{\ell}{\ell+1}} dp. \tag{39}$$

The generalized space charge limited current equations are therefore

$$i_{1,2} = \left[\frac{\epsilon\ell(1+a)}{eN_t(\ell+1)}\right]^{\ell}(\gamma N_o e\mu)\left[\frac{V^{\ell+1}}{[J_{1,2}(p_1, p_2)]^{\ell+1}}\right]. \tag{40}$$

31

We see at once from Eq. (40) that the functional dependence of the current on the voltage is the same for all three geometries as it is for the trap free and shallow trap cases. Furthermore, we see quite generally that the smaller N_t, the larger the current at any given voltage. Equation (29) shows that this is also the case for shallow trapping.

A. PLANAR GEOMETRY

We set $a = 0$ and $y = A$. The integral (39) becomes

$$J_{1,2} = \int_{p_1}^{p_2} (p - p_{1,2})^{\frac{\ell}{\ell+1}} dp = \left(\frac{\ell+1}{2\ell+1}\right)(p_2 - p_1)^{\frac{2\ell+1}{\ell+1}} \tag{41}$$

which leads to the degenerate current equation

$$i_{1,2} = \left[\frac{\epsilon \ell}{eN_t(\ell+1)}\right]^{\ell} (AN_o e\mu) \left[\frac{2\ell+1}{\ell+1}\right]^{\ell+1} \frac{V^{\ell+1}}{(p_2-p_1)^{2\ell+1}} \tag{42}$$

first considered by Rose[20,28] and later derived in detail by Mark and Helfrich[3].

B. CYLINDRICAL AND HEMISPHERICAL CONFIGURATIONS

We treat these cases together in the limit $p_2 \gg p_1$. Equation (39) evolves into the two integrals

$$J_1 \xrightarrow[p_2 \gg p_1]{} \int_{p_1}^{p_2} p^{\frac{\ell-a}{\ell+1}} dp \xrightarrow[p_2 \gg p_1]{} \left(\frac{\ell+1}{2\ell+1-a}\right) p_2^{\frac{2\ell+1-a}{\ell+1}} \tag{43a}$$

and

$$J_2 \xrightarrow[p_2 \gg p_1]{} \int_{p_1}^{p_2} p^{\frac{\ell-a}{\ell+1}} \left[\frac{p_2}{p}\right]^{\frac{\ell(a+1)}{\ell+1}} dp \xrightarrow[p_2 \gg p_1]{} p_2^{\frac{\ell(a+1)}{\ell+1}} \Gamma(p_1, p_2) \tag{43b}$$

where

$$\Gamma(p_1, p_2) = \int_{p_1}^{p_2} \left(\frac{1}{p}\right)^a dp. \tag{44}$$

Consequently

$$\left(\frac{1}{j_1}\right)^{\ell+1} = \left(\frac{2\ell+1-a}{\ell+1}\right)^{\ell+1} \left[\frac{1}{p_2}\right]^{2\ell+1-a} \tag{45a}$$

and

$$\left(\frac{1}{j_2}\right)^{\ell+1} = \left(\frac{1}{p_2}\right)^{2\ell+1-a} \left[\frac{p_2^{1-a}}{\Gamma(p_1, p_2)}\right]^{\ell+1} \tag{45b}$$

The last two equations describe the dependence of i_1 and i_2 respectively on the inter-electrode spacing. The second factor on the right side of Eq. (45b) is dimensionless as can be seen from the integral (44) for the two allowed values of a. Therefore, the currents i_2 and i_1 depend on the electrode dimensions in the same way but differ in magnitude by the ratio (rectification ratio) $\rho = i_1/i_2$

$$\rho = \left[\frac{2\ell+1-a}{\ell+1} \cdot \frac{\Gamma(p_1, p_2)}{p_2^{1-a}}\right]^{\ell+1} \tag{46}$$

which can be much larger than the ρ for the trap free and shallow trap cases because $\ell + 1$ is always greater than 2 and can be as high as 10.

We may now write down the currents and rectification ratios for both non-planar geometries under the condition $p_2 \gg p_1$.

1) Cylindrical Geometry; $a = 1$ and $\gamma = 2\pi L$:

$$i_1 = \left[\frac{2\epsilon\ell}{eN_t(\ell+1)}\right]^{\ell} (2\pi e\mu N_o L)\left[\frac{2\ell}{\ell+1}\right]^{\ell+1} \frac{V^{\ell+1}}{p_2^{2\ell}} \tag{47a}$$

33

$$i_2 = \left[\frac{2\epsilon\ell}{eN_t(\ell+1)}\right]^\ell (2\pi e\mu N_o L) \frac{V^{\ell+1}}{p_2{}^{2\ell}} \left[\ell n \frac{p_2}{p_1}\right]^{-(\ell+1)} \tag{47b}$$

$$\rho = \left[\frac{2\ell}{\ell+1} \cdot \ell n \frac{p_2}{p_1}\right]^{\ell+1} > 1. \tag{47c}$$

2) Hemispherical Geometry, $a = 2$ and $\gamma = 2\pi$:

$$i_1 = \left[\frac{3\epsilon\ell}{eN_t(\ell+1)}\right]^\ell (2\pi e\mu N_o) \left(\frac{2\ell-1}{\ell+1}\right)^{\ell+1} \frac{V^{\ell+1}}{p_2{}^{2\ell-1}} \tag{48a}$$

$$i_2 = \left[\frac{3\epsilon\ell}{eN_t(\ell+1)}\right]^\ell (2\pi e\mu N_o) \frac{V^{\ell+1}}{p_2{}^{2\ell-1}} \left(\frac{p_2}{p_1}\right)^{-(\ell+1)} \tag{48b}$$

$$\rho = \left[\frac{2\ell-1}{\ell+1} \cdot \frac{p_2}{p_1}\right]^{\ell+1} > 1. \tag{48c}$$

We note that ρ is always greater than unity. Hence the i_1's are the "forward" currents and the i_2's are the "reverse" currents. We also see a similarity between the ρ's for the trap free, shallow trap and exponential trap cases. For the cylindrical geometry, the ρ's contain the factor $\ell n(p_2/p_1)$ while the hemispherical geometry involves the ratio p_2/p_1.

If we relax the condition $p_2 \gg p_1$, the integrals (15) and (39) become more complicated and may even not be solvable in closed form. However, because of the way these integrals appear in the generalized currents, the actual values of these integrals will not affect the functional dependence of the current on the voltage. Their values will influence both the magnitude of the currents and the rectification ratios.

7. SOME GENERAL CONSIDERATIONS

The results of this analysis are summarized in Table IV-1. There is a very general symmetry among these equations and it might be expected that the analysis is even more general than we have indicated in this treatment. This is indeed the case mathematically although the physical significance of a further mathematical generalization is somewhat dubious. We can, however, quite generally assert the following. If the function f (Eq. (5)), which expresses the relation between the total injected carrier concentration and the free carrier concentration can be written most generally as a product of two functions

$$K \cdot f_1(i) \cdot f_2 \left(\frac{1}{p^a \mathcal{E}(p)} \right) \tag{49}$$

where K is a constant involving N_o, N_t, e, ϵ, γ and μ and where f_1 and f_2 are not necessarily the same functions, then the functional dependence of the generalized current on the applied voltage will be determined by the trap distribution and will not depend on the electrode geometry. This follows from the fact that the two integrations involved in the solution of Eq. (8), first to obtain the field and second to obtain the potential, do not affect the function f_1 in (49) which contains the current. This function is merely a constant during these integrations. It is clear that this condition has been satisfied for the three choices of f in this analysis which may be written formally as $f = 1$, $f = 1/\theta$ and $f = (N_t/N_o^{1/\ell})$ [   ]$^{1/\ell}$ for the trap free, shallow trap and exponential trap cases respectively.

We may also estimate the current levels expected from a material with an exponential trap distribution. In general, these are unfortunately rather low for the non-planar electrode geometries where rectification is expected. However, the currents are very sensitive to N_t and ℓ. Very generally, one might expect currents of the order of 10^{-9} to 10^{-5} amps over a voltage range from 1.0 to 100 volts. For the planar cases, the currents can be quite large as the literature amply demonstrates[5] but here no rectification occurs. The non-planar configurations may find some practical applications in very high impedance devices. Equally important, however, non-planar configurations may be valuable for less technical applications. For example, it is possible to determine whether a particular electrode material is ohmic for hole or electron injection by measuring $i_{1,2}$ using a non-planar geometry first with the "unknown" ohmic contact on one side, say p_1, and a known blocking contact on the other side p_2 and then by repeating the experiment with the contacts interchanged.

TABLE IV-1

SUMMARY OF RESULTS

ELECTRODE CONFIGURATION	TRAP FREE AND SHALLOW SINGLE TRAP LEVEL [θ]*		EXPONENTIAL TRAP DISTRIBUTION	
	i	ρ	i	ρ
plane-parallel	$i_{1,2} = \dfrac{9}{8}\epsilon\mu A\,\dfrac{V^2}{(p_2-p_1)^3}[\theta]$	—	$i_{1,2} = \left[\dfrac{e}{eN_t(\ell+1)}\right]^{\ell}(e\mu N_o A)\left[\dfrac{2\ell+1}{\ell+1}\right]^{\ell+1}\dfrac{V^{\ell+1}}{(p_2-p_1)^{2\ell+1}}$	—
cylindrical	$i_1 = 2\pi\epsilon\mu L\,\dfrac{V^2}{p_2^2}\,[\theta]$ $i_2 = i_1\left[\ln\dfrac{p_2}{p_1}\right]^{-2}$	$\left[\ln\dfrac{p_2}{p_1}\right]^2$	$i_1 = \left[\dfrac{2e\ell}{eN_t(\ell+1)}\right]^{\ell}(2\pi e\mu N_o L)\left[\dfrac{2\ell}{\ell+1}\right]^{\ell+1}\dfrac{V^{\ell+1}}{p_2^{2\ell}}$ $i_2 = i_1\left[\dfrac{2\ell}{\ell+1}\cdot\ln\dfrac{p_2}{p_1}\right]^{-(\ell+1)}$	$\left[\dfrac{2\ell}{\ell+1}\cdot\ln\dfrac{p_2}{p_1}\right]^{\ell+1}$
hemispherical	$i_1 = \dfrac{3\pi}{4}\,\epsilon\mu\,\dfrac{V^2}{p_2}\,[\theta]$ $i_2 = i_1\left[\dfrac{p_2}{2p_1}\right]^{-2}$	$\left[\dfrac{p_2}{2p_1}\right]$	$i_1 = \left[\dfrac{3e\ell}{eN_t(\ell+1)}\right]^{\ell}(2\pi e\mu N_o)\left[\dfrac{2\ell-1}{\ell+1}\right]^{\ell+1}\dfrac{V^{\ell+1}}{p_2^{2\ell-1}}$ $i_2 = i_1\left[\dfrac{2\ell-1}{\ell+1}\cdot\dfrac{p_2}{p_1}\right]^{-(\ell+1)}$	$\left[\dfrac{2\ell-1}{\ell+1}\cdot\dfrac{p_2}{p_1}\right]^{\ell+1}$

* The factor $[\theta] = 1$ for the trap free case and is given by Eq. (29) for the single shallow trap case.

V. SOME ELECTRICAL PROPERTIES OF THE ARSONIUM SALT
OF TETRACYANOQUINODIMETHANE

1. INTRODUCTION

The search for a novel contact to insulators was begun by examining some of the electrical properties of the organic ion radical salt. arsonium salt of tetracyanoquinodimethane, which is written symbolically as $As,-(TCNQ)$. This material was prepared in the duPont Research Laboratories [31] and was supplied from this source. The substance has the composition[32] $CH_3(C_6H_5)_3 As^+(TCNQ)^- (TCNQ)^o$ where TCNQ has the structural formula[32]
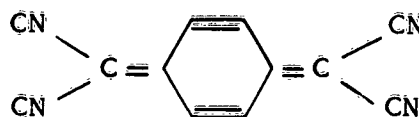
The material can be prepared as a single crystal[32,33] (monoclinic), the conductivity of which is remarkably high for an organic substance and very anisotropic.[33,34] The TCNQ units are arranged in infinite face-to-face stacks with the direction of highest conductivity $(2 \times 10^{-2}$ ohm^{-1} cm$^{-1})$ normal to the plane of the TCNQ. The conductivities along the other two crystal directions are 2×10^{-3} ohm^{-1} cm^{-1} and 5×10^{-5} ohm^{-1}cm^{-1}. The crystals are black, rather soft and have a sharp melting point at 225°C[32] at which temperature a slight decomposition in air was observed. The conductivity follows an Arrhenius temperature dependence $(\sigma = \sigma_o\, e^{-A/kT})$ with an isotropic activation energy $A = 0.33$ ev.[34] The thermoelectric power is positive at low temperature, passes through zero near 300°K, and remains negative up to the melting point.[34] Along the direction of highest conductivity, the duPont group reports the value -50 μvolts/°C at 25°C from which they conclude that the material is n-type. A Hall mobility measurement for the arsonium salt is not reported in the literature. However an unsuccessful attempt by the duPont group to observe a Hall voltage in a similar salt, the trimethylammonium salt of TCNQ, yielded an upper limit of 0.04 cm²/volt sec for the mobility.[35]

This material is an interesting candidate as an injecting contact to insulators because of some similarities with certain electrolytic electrodes[3,6,36](iodide salt solutions saturated with iodine) and a CuI electrode[37] (actually a solid solution of iodine in CuI) both of which

form injecting contacts for holes to a variety of molecular crystals.[3,6,36,37] They are salts (and CuI is also a p-type semiconductor), they have high conductivity, higher than the insulator to which they must form contact, and they contain strong electron acceptors (dissolved iodine or the TCNQ molecule). For this reason, the following experiments were performed in an effort to learn more about the electrical and contact properties of As-(TCNQ). Point contact measurements with crystals of As-(TCNQ) were made to determine the carrier sign. Next, the behavior of a contact between As-(TCNQ) and an evaporated n-type CdS layer was examined. Finally a Hall effect measurement was attempted. The results of these three experiments can be briefly summarized. From the point-contact measurements and the behavior of the As-(TCNQ)-CdS junction, it can be concluded that As-(TCNQ) behave as a p-type semiconductor at room temperature. No Hall voltage was observed, which indicates that the mobility was at most $0.1 \text{ cm}^2/\text{volt sec}$ on the assumption of one-carrier conductivity and that carrier transport can be described by a crystal band scheme. These conclusions are discussed in greater detail after the experiments have been described.

2. POINT-CONTACT MEASUREMENTS

The tungsten point-contacts were made by electrolytic etching.[38] A 1.0 M NaOH solution served as the electrolyte and a nickel wire was used as the other electrode. The system was driven at 10 volts (rms) 60 cps for about two minutes to produce points of sub-micron dimensions on 15 mil tungsten wire. The As-(TCNQ) crystal (about 2mm linear dimensions) was mounted on a glass slide and affixed to it with silver paste which also served as the ohmic base contact[34]. The tungsten point was brought in contact with the top surface of the crystal which was oriented in such a way that the field was essentially parallel with the axis of medium conductivity.

Figure V-1 illustrates the dynamic (40 cps) current-voltage characteristic of the As-(TCNQ) point contact system. Rectification is clearly evident, the reverse direction occuring with the point positive with respect to the base. At higher measuring frequencies characteristic looping of the current was observed as were breakdown phenomena at higher voltages.

Figure V-2 illustrates the static current-voltage characteristic measured with another crystal. Here again, there is clear evidence of rectification and the reverse direction also occurs with the point at positive bias. The ohmic region at the high voltage end of the forward current is caused by spread resistance limitations. The reverse breakdown voltage was about 50 volts for both the dynamic and static measurements.
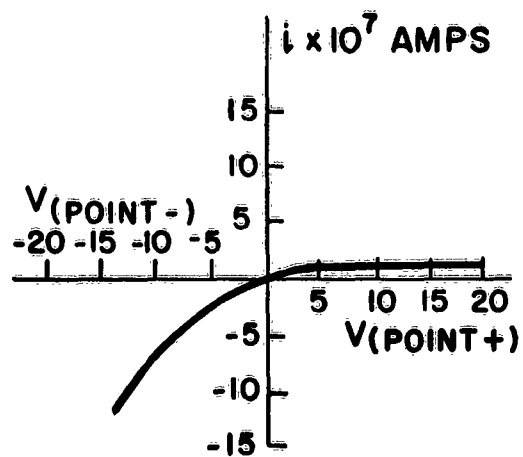
FIG. V-1 DYNAMIC (40 CPS) CURRENT-
VOLTAGE CHARACTERISTIC OF
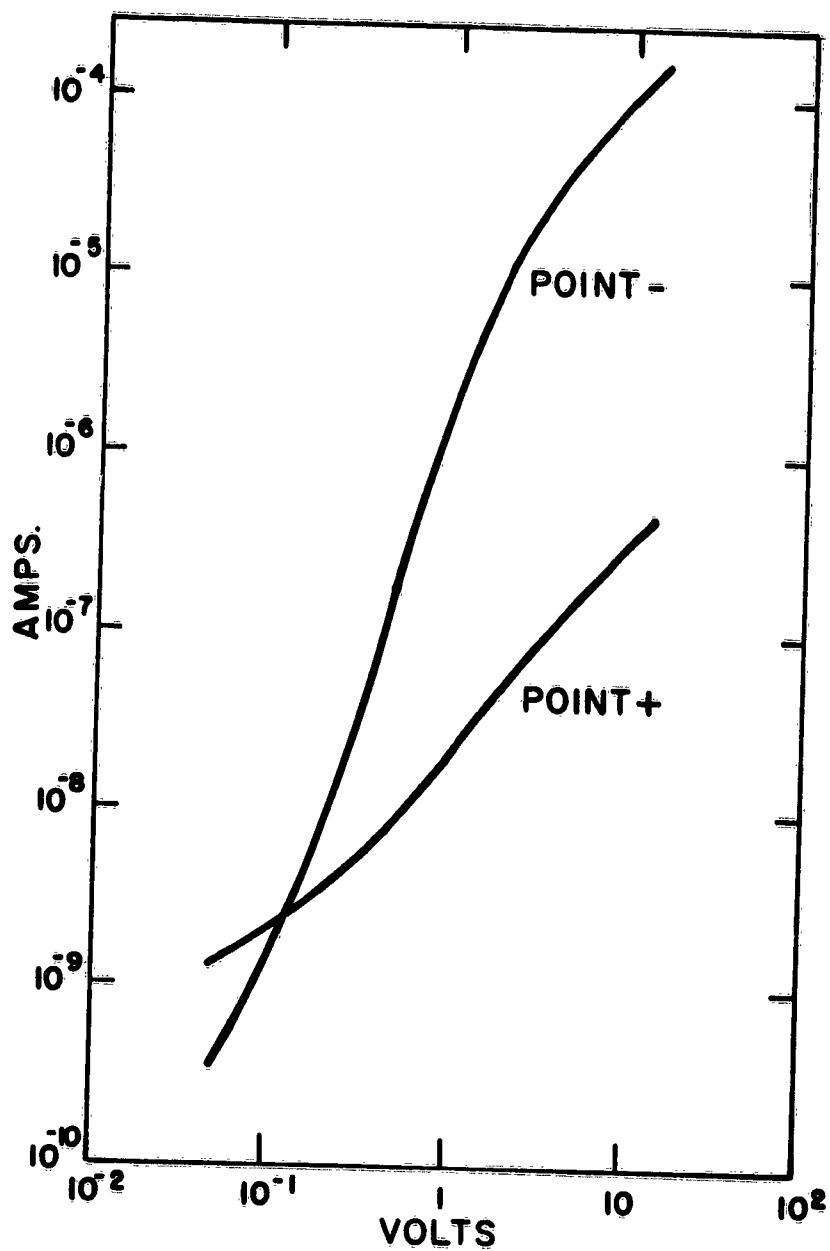TUNGSTEN POINT ON As, (TCNQ)

FIG. V-2   STATIC CURRENT – VOLTAGE
CHARACTERISTIC OF TUNGSTEN
POINT ON As,(TCNQ)

40

3. CONTACTS TO CdS

The contact between As-(TCNQ) and an evaporated n-type CdS film was also examined. The CdS film, which was 5 microns thick, made contact to an evaporated transparent Au electrode on a glass substrate. The resistivity of the film was about 10^4 ohm cm. The As-(TCNQ) crystal was melted onto the film at 225°C and allowed to solidify. The contact area was about 0.25 cm^2. A tungsten wire was jammed into the solidified As-(TCNQ) to complete the circuit. The As-(TCNQ) was melted onto the CdS to provide good mechanical contact. The solidified melt appeared to consist of recrystallized regions; it was essentially polycrystalline. Surprisingly, the conductivity behavior of the solidified melt was very similar to that of the single crystal. Point-contact measurements with the solidified melt also show rectification with reverse current flow occurring when the point is at positive bias.

In the dark, the As-TCNQ-CdS junction exhibited a small open circuit voltage: 0.035 volt with As-(TCNQ) negative with respect to the CdS. The static dark current-voltage characteristic of the junction is shown on Fig. V-3. Considerable rectification is clearly evident with the forward direction occurring when the As-(TCNQ) was positive with respect to the CdS film. Between 1 and 10 volts, the rectification ratio is greater than 100. The maximum rectification occurred at two volts, where it was just under 10^3. The ohmic region at the high voltage end of the forward current corresponds to the resistance of the As-(TCNQ).

Similar experiments were repeated with the junction illuminated through the CdS film with unfiltered light from a microscope illuminator. An intensity-dependent photovoltage was observed with the As-(TCNQ) now positive with respect to the CdS. Under maximum illumination, the magnitude of the photovoltage was 0.25 volts. Figure V-4 illustrates the static current-voltage characteristic of the junction under maximum illumination. Consider first the forward current (TCNQ+). The high voltage region coincides with the forward dark current. As the forward voltage is reduced towards 0.25 volts, the current begins to drop below the dark current and passes through zero current at 0.25 volts. This occurs because the photovoltage acts to buck out the applied voltage. At forward voltage less than the photovoltage, the current opposes the applied voltage. The reverse current (TCNQ-) exceeds the forward current below 0.5 volts, is practically ohmic and is much larger than the reverse dark current, although the two reverse currents tend to merge at high voltage. The large reverse current under illumination is, in all likelihood, caused by the photoconductivity of the CdS film. The reverse breakdown voltage under illumination is less than in the dark

41
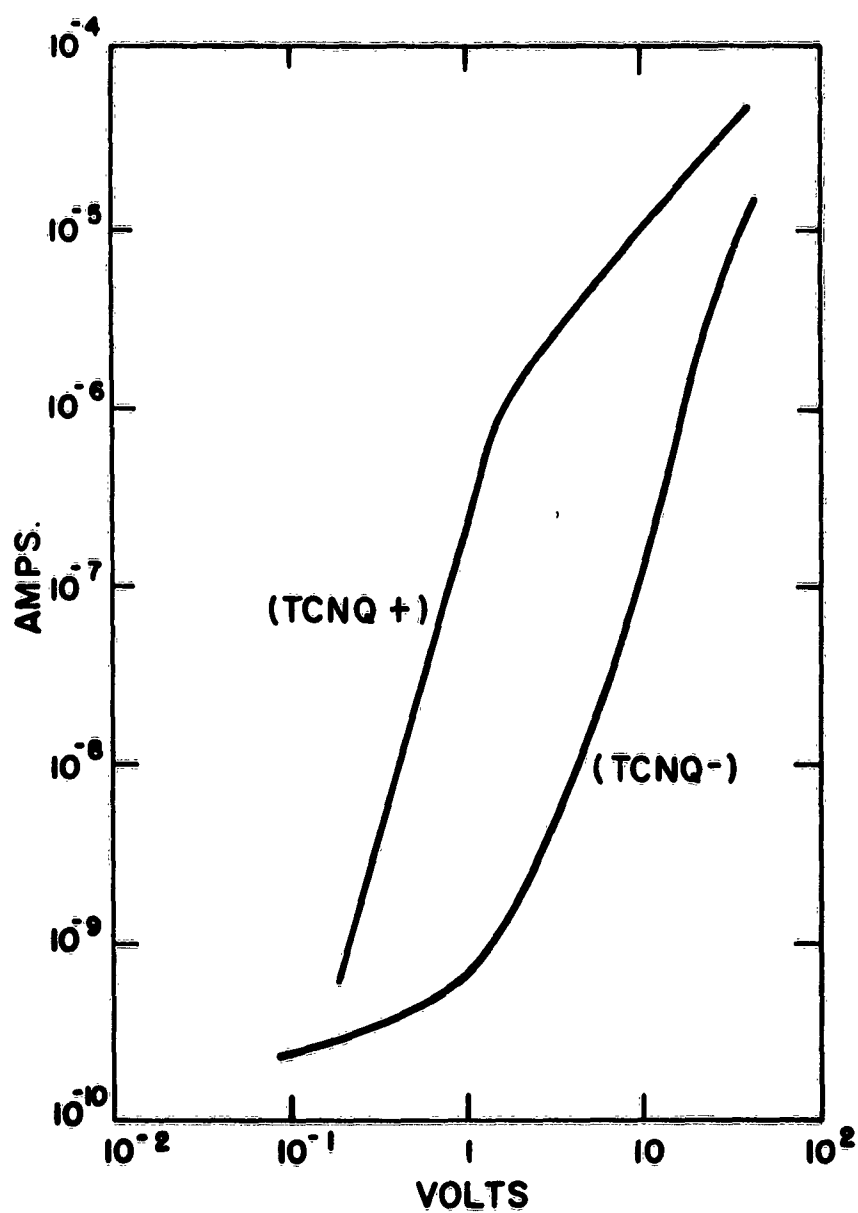
FIG. V-3   DC CURRENT- VOLTAGE
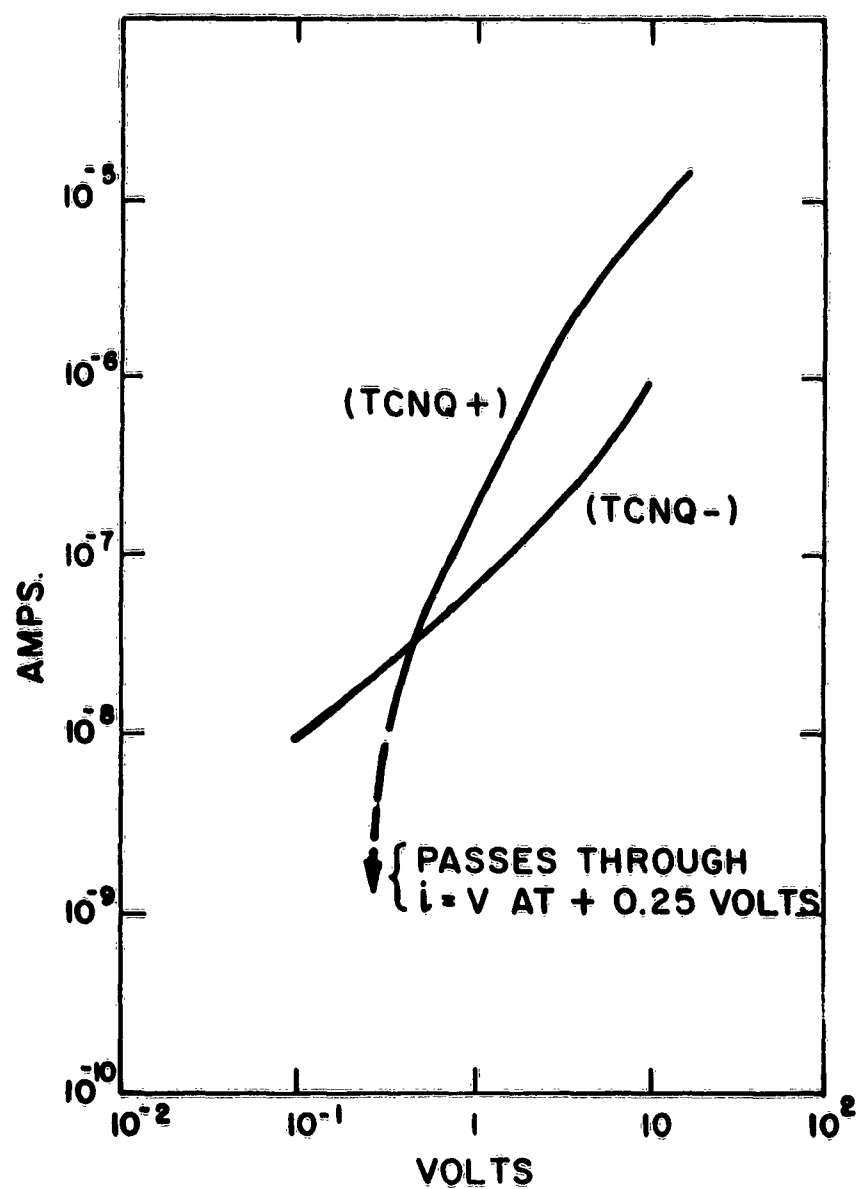CHARACTERISTICS OF CdS-As,
(TCNQ) CONTACT IN THE DARK

42

FIG. V-4   DC CURRENT – VOLTAGE
CHARACTERISTICS OF CdS – As,
(TCNQ) CONTACT UNDER
ILLUMINATION WITH WHITE
LIGHT

43

(this is why the reverse current under illumination was not measured to high voltages). This is caused by the increased conductivity of the CdS layer which causes a higher field to appear across the junction.

4. HALL EFFECT

A Hall effect measurement on a crystal of As-(TCNQ) was also attempted. Silver paste was used for both the end contacts and for the Hall probes. No Hall voltage was observed for magnetic fields up to 6000 gauss. If one assumes one-carrier conduction and a conventional energy band scheme to describe the carrier transport (which is unlikely in this material), the sensitivity of the apparatus (see Sec. II) dictates that the carrier mobility is at most 0.1 cm^2/volt sec.

5. QUALITATIVE DISCUSSION

The major conclusion which may be drawn from these experiments is that As-(TCNQ) behaves as a p-type semiconductor. The point contact rectification polarity shows this most clearly. Reverse direction with the point positive is a typical characteristic of a p-type semiconductor[39,40]. The junction with the n-type photoconducting CdS behaves as a p-n junction.[40] The diffusion of holes from the p-region (TCNQ) to the n-region in the dark can account for the polarity of the open circuit voltage in the dark. The polarity of the photovoltage also fits in with this interpretation. The current-voltage characteristics are also qualitatively in accord with p-n junction theory[40]. At present, the measurements are not sufficiently complete for quantitative interpretation. The junction is also more complicated than those usually encountered in practice because it has been formed from two different materials: a wide band-gap n-type material (CdS) and a lower band-gap p-type material. Also it is unlikely that carrier transport in As-(TCNQ) can be realistically described by a conventional band model[41] (i.e. with the free carriers moving in bands of width much greater than kT). It may even be that carrier transport occurs by tunneling[11] or by phonon-assisted charge transfer[10]. Nevertheless, this material does have properties typical of a p-type semiconductor quite similar to the CuI electrode material mentioned before. Its behavior as an electrode contact to various insulators will be studied further.

One additional potentially interesting feature of the electrical behavior of As-(TCNQ) is worth emphasizing: the change in the sign of the thermoelectric power Θ at room temperature. Along the axis of highest conductivity, the duPont group reported the value $\Theta = -50 \ \mu v/°C$, characteristic of an n-type carrier.[42] The duPont measurement could then be interpreted to

44

mean that along the highest conductivity direction, As-(TCNQ) is n-type at room temperature. But the room temperature reported here indicate the opposite for the solidified melt and along the medium conductivity direction for the single crystal. Also a change in the sign of Θ near room temperature would imply that it should be possible to modulate the conductivity type with the temperature. However, this conventional association of the sign of Θ with the conductivity type is subject to misinterpretation. Inhomogeneities in the material can easily cause this association to fail. It is therefore necessary to measure the carrier sign directly. Unfortunately, the Hall measurement was inconclusive and the time-of-flight measurement may prove difficult because of the high conductivity (short dielectric relaxation time) of the material[43,44]. Nevertheless, a time-of-flight measurement will be attempted.

VI. PHOTOCONDUCTIVITY IN CUBIC CdS

All of the existing data on photoelectronic properties of cadmium sulfide have been obtained for the hexagonal crystal form. This situation results from the instability of the cubic form at temperatures sufficiently high to make single crystals, or even photoconducing layers or powders by conventional methods. We report here measurements on a cubic cadmium sulfide powder prepared by precipitation of cadmium methyl mercaptide by reaction between methyl mercaptan and cadmium acetate solution, followed by sufficient heating to decompose the mercaptide.

If one of the hydrogens in H_2S is replaced by an organic group, a class of compounds known as mercaptans is formed. The lowest member of this series is CH_3SH, methyl mercaptan. Since both hydrogens in H_2S are ionized to some extent, the hydrogen bonded to sulfur in CH_3SH is also ionized sufficiently to form a weak acid in aqueous solution. This allows the preparation of salts known as mercaptides, analogous to salts formed from H_2S.

Milligan[45] and Rittner and Schulman[46] have described the effect of precipitation conditions on the crystal structure of CdS prepared by precipitation with H_2S. CdS precipitated from an acid solution of $CdSO_4$ was largely cubic, whereas CdS precipitated from $CdCl_2$ was largely hexagonal. The salt of CH_3SH, which corresponds to CdS as the salt of H_2S, is cadmium methyl mercaptide $Cd(SCH_3)_2$. This compound may be regarded as CdS with the Cd-S bond modified by the methyl group bonded to the S.

$Cd(SCH_3)_2$ was prepared from a 0.1 M cadmium acetate solution by bubbling CH_3SH slowly through the solution. The system was first completely flushed with nitrogen to prevent the air oxidation of CH_3SH. $Cd(SCH_3)_2$ was formed as a semicrystalline white precipitate which was found to be insoluble in a variety of organic solvents. Partial purification was effected by repeated washings with hot water followed by drying in a vacuum oven at 115°C. The identity of the precipitate was established by chemical analysis.[47]

$Cd(SCH_3)_2$ decomposes on heating to form CdS and volatile $(CH_3)_2S$, this decomposition occurring at about 198°C. Table VI-1 summarizes the characteristics of the precipitate obtained by the above procedure, after heating to 250° and to 800°C, and these are compared with those of precipitated CdS (RCA 33C291A) heated to these same temperatures.

TABLE VI-1

*DATA RELEVANT TO THE PROPERTIES
OF CUBIC CdS*

DESCRIPTION OF SAMPLE	BODY COLOR	X-RAY ANALYSIS*	PHOTOELECTRONIC PROPERTIES
Unheated $Cd(SCH_3)_2$	White	Complex organic crystalline	Inert
$Cd(SCH_3)_2$ heated to 194°C	Yellow	Same as unheated sample	Inert
$Cd(SCH_3)_2$ heated to 250°C	Reddish	Cubic and hexagonal CdS; major phase cubic	Figure VI-1; Curve 1
CdS heated to 250°C	Yellow	Hexagonal and cubic CdS; major phase hexagonal	Figure VI-1; Curve 3
$Cd(SCH_3)_2$ heated to 800°C	Dark Brown	Hexagonal CdS	High conductivity[†] (cell resistance = $10^4 \Omega$
CdS heated to 800°C	Yellow	Identical with above hex.-CdS	High conductivity[†] (cell resistance = $10^7 \Omega$
$Cd(SCH_3)_2$ heated to 450°C	Brown		Figure VI-1; Curve 2

*X-ray analysis by R. J. Paff

[†]Dark conductivity of other cells in this table $\geq 10^{12} \Omega$

Three photoconductivity spectral response curves are shown in Fig. VI-1. These were measured for the powder mixed with a binder of ethyl cellulose in amyl acetate and measured on a gap cell according to standard techniques.[48,49] Curves 1 and 2 are for the CdS as prepared in this paper, after firings at 250° and 450°C respectively. The sample fired at 250°C is principally cubic and indicates a band gap of about 2.1 ev. This same sample after firing to 450°C has largely converted to the hexagonal form and shows the same band gap of about 2.4 ev typical of the precipitated CdS, as illustrated by curve 2 for precipitated CdS fired to 250°C. We believe that this is the first photoelectronic indication of the band gap in cubic CdS.
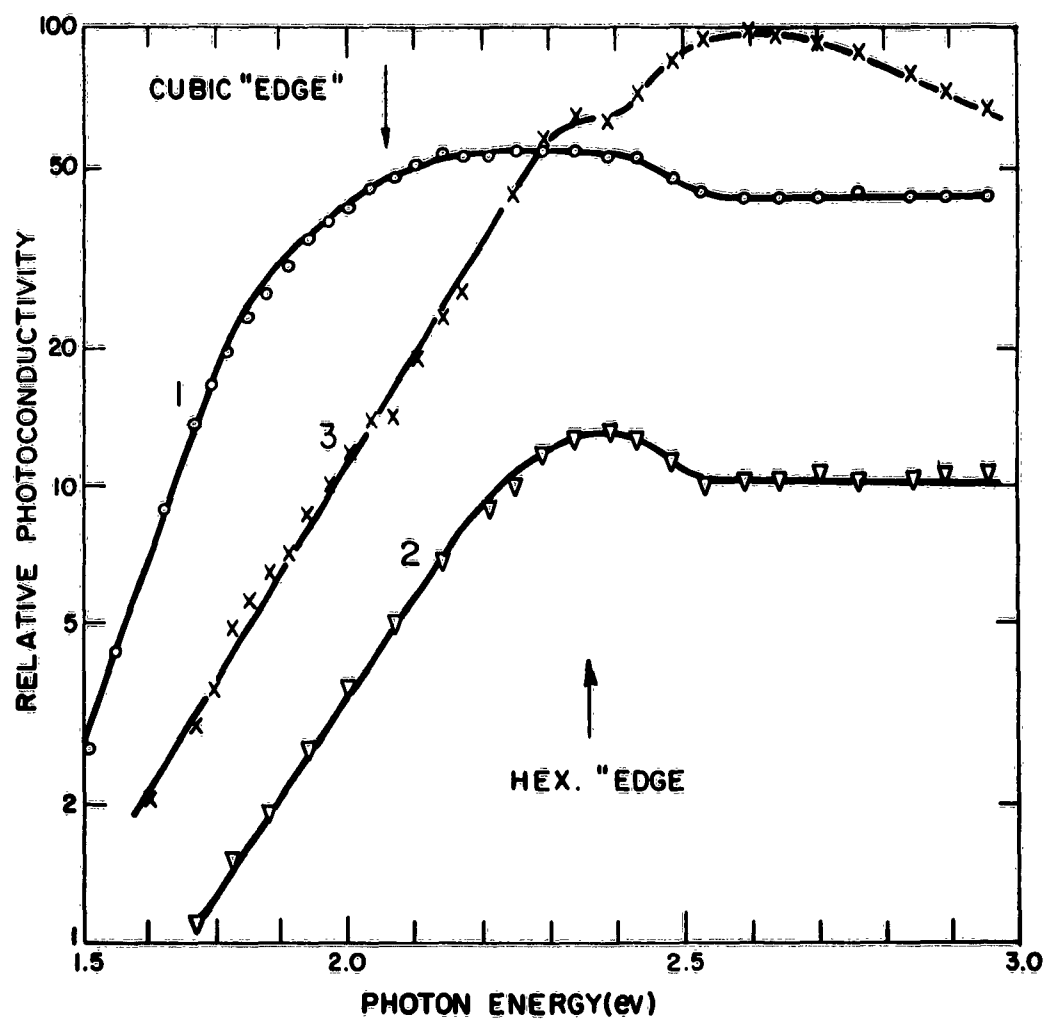
47

FIG. VI-1

48

VII. PREPARATION OF MATERIALS

1. INTRODUCTION

During the period covered by this report, the program was modified to include the preparation and measurement of charge transport properties of insulators other than CdS. These materials include elemental Se and organic compounds such as anthracene for reasons given elsewhere in this report. The work on CdS, therefore, proceeded at a reduced rate while the new experiments were initiated.

2. SUBLIMATION IN A MOVING-TEMPERATURE GRADIENT — CdS, CdS:Cu, CdS:Ag and CdS:Au

This method for producing large single crystal boules was described in Section II-4 and Fig. 6 of Report No. 2; the photoelectronic analysis of a number of boules was presented in Section IV-1 of that report. The cylindrical axis of these bullet shaped samples is the growth axis, but it has been found by X-ray diffraction analysis (performed by G. Neighbor) that this growth axis is often neither parallel nor perpendicular to the crystal c-axis. Different orientations have been found in five different samples with the angle between the two axes ranging between 5° to 70° inclusive. Previously it had been noted that the tip angle of the growth tube had no apparent influence on the crystallinity of a boule, and, for the present there is also no correlation between this angle and the axial orientations. It appears that nucleation and subsequent crystal growth are random with respect to this axial relationship. It is possible, however, that nucleation occurs initially with the c-axis in a preferred direction which changes at some point in the growing crystal perhaps as a consequence of dislocations or other crystal defects. Sulfur vacancies, for example are believed to be responsible for the high conductivities observed in many of the boules.

In this connection a number of samples from these high conductivity boules were cut and polished in preparation for chemical etching and other experiments. A preliminary check of their conductivities disclosed that one sample had a very high resistivity whereas another slice from this same boule previously had been found to be quite conducting. This inhomogeneity may be due to crystal defects or to a local segregation of a chemical impurity.

The preparation of CdS:Cu boules was described in the previous report. Spectrochemical analyses for copper (by K. L. Cheng) have now shown that the copper is probably not uniformly distributed throughout the boule. Transmission data from cut and polished samples of equal

49

thickness confirm this. No detectable Hall voltage could be found in a specimen from one boule. Some evidence, however, that the conductivity may be p-type was obtained from the observation that another portion of the same boule with clearly less Cu (by measurement of transmission) was many orders of magnitude higher resistivity. These measurements and the transmission data have been described by Bube, Lind and Dreeben[50].

Similar boules doped with Ag and Au have also been grown by addition of appropriate sulfides to the CdS charge. The boule resulting from the addition of 1.3 mole% Ag to the charge was black in color, but 2 mole% Au could not be so detected visually. In the latter case only a low amount may be incorporated in the boule as a result of losses from easily decomposed Au_2S. The growth of this boule, however, seemed more rapid, perhaps because gold actually enhances the growth mechanism, or because the system $CdS:Au_2S$ has a higher vapor pressure at the growth temperature than does CdS alone. The boule exhibited many grain boundaries which is consistent with too rapid a growth rate. The Au impurity itself with a larger radius than Cd may also inhibit the formation of large single crystals. Spectrochemical analyses showed that as noted for Cu, the Ag and Au impurities are also inhomogeneously distributed in the boules.

X-ray diffraction examination (by R. J. Paff) of a number of samples from various boules showed only hexagonal CdS in all cases. No differences could be found in c/a ratios even in samples containing high concentrations of Cu. A second phase of Cu_2S was not detected, but the amount of Cu_2S in this case was near the lower limit of X-ray detection.

3. SUBLIMATION IN A STATIC SYSTEM – CdS

Using the procedures previously described (Report No. 2, Section II-2), polycrystalline ingots of pure CdS, 1.5 inches in diameter and up to 0.5 inches thick have been grown in an Ar atmosphere at temperatures between 1070-1200°C. Single crystal areas up to 100 mm^2 can be recovered from these ingots. The technique can probably be improved to yield larger pieces.

Heretofore in the static method, the crystals of CdS nucleated and grew around the walls of the growth tubes. In an effort to control the growth process better, two different techniques to limit nucleation sites have been tried. In one, quartz discs with their faces perpendicular to the long axis of the growth tube were positioned at intervals in the usual growth region of the tube. It was found that in an H_2S atmosphere and a temperature gradient of the type shown in Fig. 2b, page 6, Report No. 2, polycrystalline mats deposit on the faces of the discs. The thickness of the deposits apparently depends on the substrate

temperature, and to some extent on the geometry of the arrangement. It is interesting that no deposition or growth occurred around the walls of the growth tube or on the periphery of the discs.

In the second procedure the discs were replaced by single thin quartz fibers. With this configuration, the usual assortment of crystal habits are produced on the walls of the tube as well as on the fibers where twinning is also common. The results are encouraging with respect to the aim of limiting nucleation sites enabling large plate-like crystals to grow from one or two positions on a fiber. The shape of the temperature gradient is likely to be a critical factor in achieving this result.

4. CRYSTAL GROWTH OF SELENIUM

Elemental Se, with a melting point of 218°C exists in many different allotropic forms. These include two red monoclinic varieties, grey and black hexagonal forms, and several red and black amorphous modifications. The various forms exhibit differences in chemical and physical properties such as solubility, density and electrical conductivity as well as crystal structure[51-53]. The grey hexagonal form consists of "zig zag" chains of Se^{54}.

The existence of these many allotropic forms creates problems in growing single crystals of Se. Growth from the melt and also from the vapor phase, however, have been accomplished, one of the more recent efforts being reported by Kosgrev[55] who required two months of continuous operation to grow 15×7×6 mm crystals from the vapor phase. This slow rate of growth was attributed to the necessity for opening the chain molecules of amorphous selenium to supply the molecules for the growing crystal.

In the present work emphasis has been on growth from the vapor. Crystals of Se up to 2×5×0.4 mm have been grown by sublimation in vacuo at 170-200°C in 1-2 weeks with the Se charge held at about 240°C. In addition to these plates and needles, there were some with a foliated habit. Typical samples are shown in Fig. VII-1.

The grey hexagonal modification was strongly suggested by the appearance and growth conditions of the crystals. X-ray diffraction examination of several samples by transmission Laue technique (performed by W. C. Roth) showed that the specimens were crystalline with an axis of symmetry, but the hexagonal structure could not be uniquely inferred from the Laue photographs alone. Some lattice deformation was evidenced by streaks instead of spots on the photographs. Such deformation can easily occur after

51
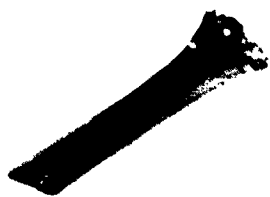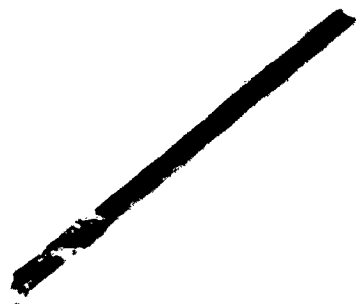
FIG. VII-1

growth because the crystals are quite plastic being easily distorted to a new permanent shape without breaking. This property has also been observed by Hyman[56] who accounts for it in terms of dislocations and bending about the axis perpendicular to the c-axis. These facts serve to emphasize the importance of careful post-growth-handling of Se crystals and suggest that annealing procedures may be useful to relieve strains.

5. CRYSTAL GROWTH OF ANTHRACENE

Anthracene is one of several organic compounds whose electrical properties are to be studied. As a result of recent interest in these properties, modified crystal growing procedures have been reported. Ferguson and Schneider[57], and Mark[58] used sublimation methods, while Kallman and Pope[59] employed a novel procedure for growth from solution. Lipsett[60] describes additional techniques for both of these methods, and in addition reports the growth of large crystals from the melt by the Bridgman method.

In the present work, all of these procedures are being utilized. Growth from solution is relatively easy to initiate but requires careful adjustment of concentration and cooling or evaporation rates. Plate-like crystals, examples of which are shown in Fig. VII-2 have been produced by slow cooling of a solution containing about 15 g of anthracent in 100 ml of N,N-dimethylformamide. Either this procedure or that of Kallman and Pope[59] can supply crystals adequate for some electrical measurements. One drawback is the possible unknown influence on properties of solvent trapped or incorporated in the crystals.

In order to avoid problems connected with the presence of a solvent, the moving gradient technique has been applied to the growth of anthracene by sublimation. (The experimental technique has been described in Report No. 2 in connection with its successful application to CdS. Briefly it consists of having a temperature gradient move slowly over a material contained in a horizontal growth tube with a pointed tip so that the maximum temperature causes the material to sublime. The tip of the growth tube is initially at a temperature too high for condensation of the vapors to occur, but as the gradient advances, the tip cools, and at some point nucleation occurs and a crystal grows.)

The growth tube, containing a pre-melted piece of anthracene is positioned in the furnace so that the tip is initially 3-8° lower than the maximum temperature. The system is evacuated and flushed with argon prior to heating. T_{max} has been varied in different experiments from just below the melting point of anthracene (218°C) to 170°C. In all cases the anthracene sublimed to form a milky white polycrystalline boule with small grains. As T_{max} has been reduced, however, a small portion of the boule near the tip has become
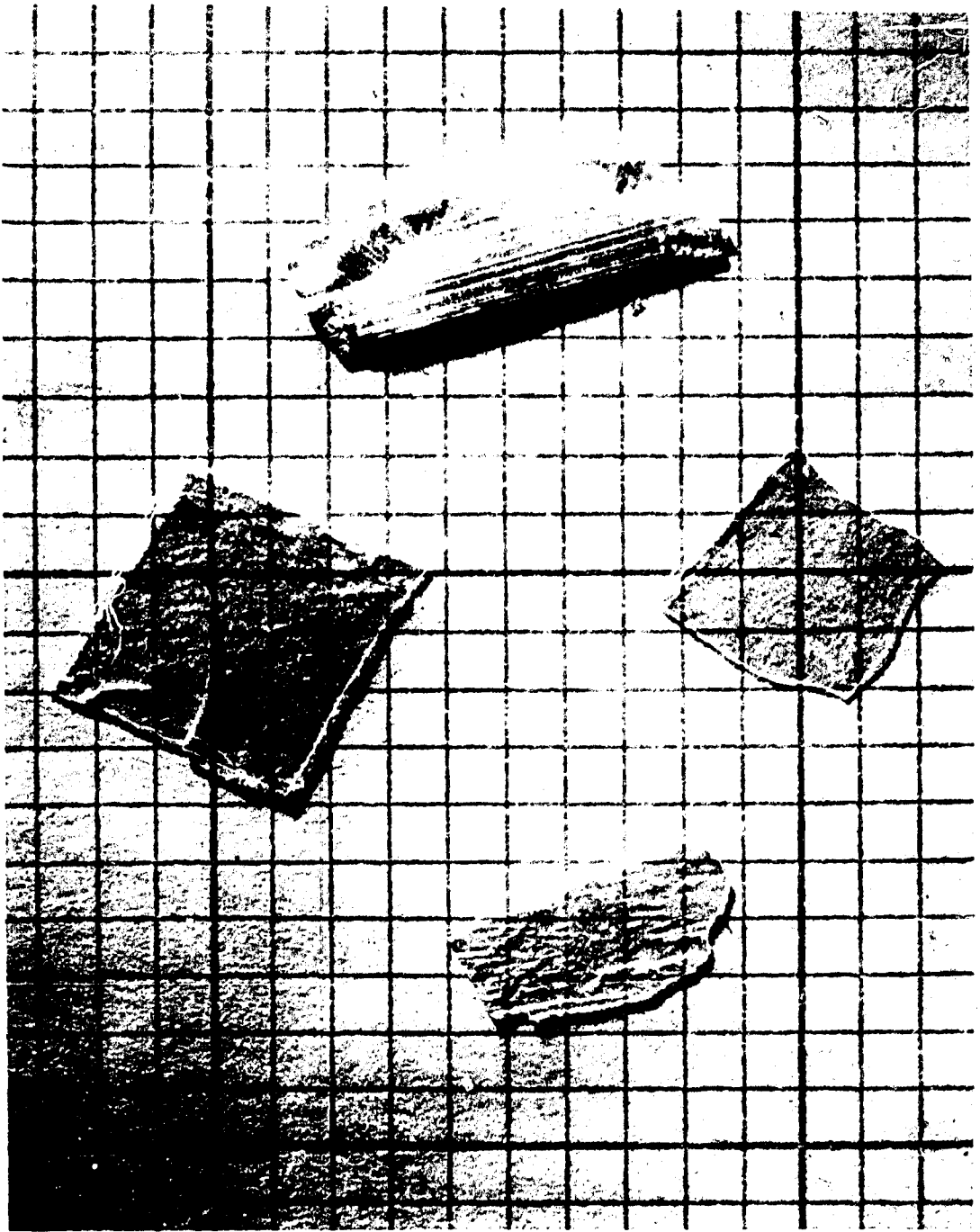
53

FIG. VII-2

transparent, thus offering encouragement that a boule with large single crystal areas can be grown by this method under the proper conditions.

Growth from the melt by the Bridgman method will be accomplished in a recently constructed furnace shown in Fig. VII-3. It consists of two independently controlled temperature zones to permit flexibility in establishing suitable temperature gradients. The nichrome wire wound Alundum core is enclosed in Fiberfrax insulation. Also shown is a typical temperature gradient which can be maintained within $\pm 0.5°$ by proportional controllers. The growth ampoule, shown in its initial position in the furnace, is loaded with powdered anthracene (Eastman Kodak, blue-violet fluorescent grade) and evacuated to a pressure less than 10^{-5} torr. and sealed off. The support wire is led to a shaft turned by a synchronous motor. At present the ampoule is lowered through the gradient at a rate of 0.075 inches per hour, until all of the sample is below the melting point. Under the most favorable conditions, the portion of the sample above the constriction may be a single crystal or have at most a few large single crystal areas. These conditions are now being determined.
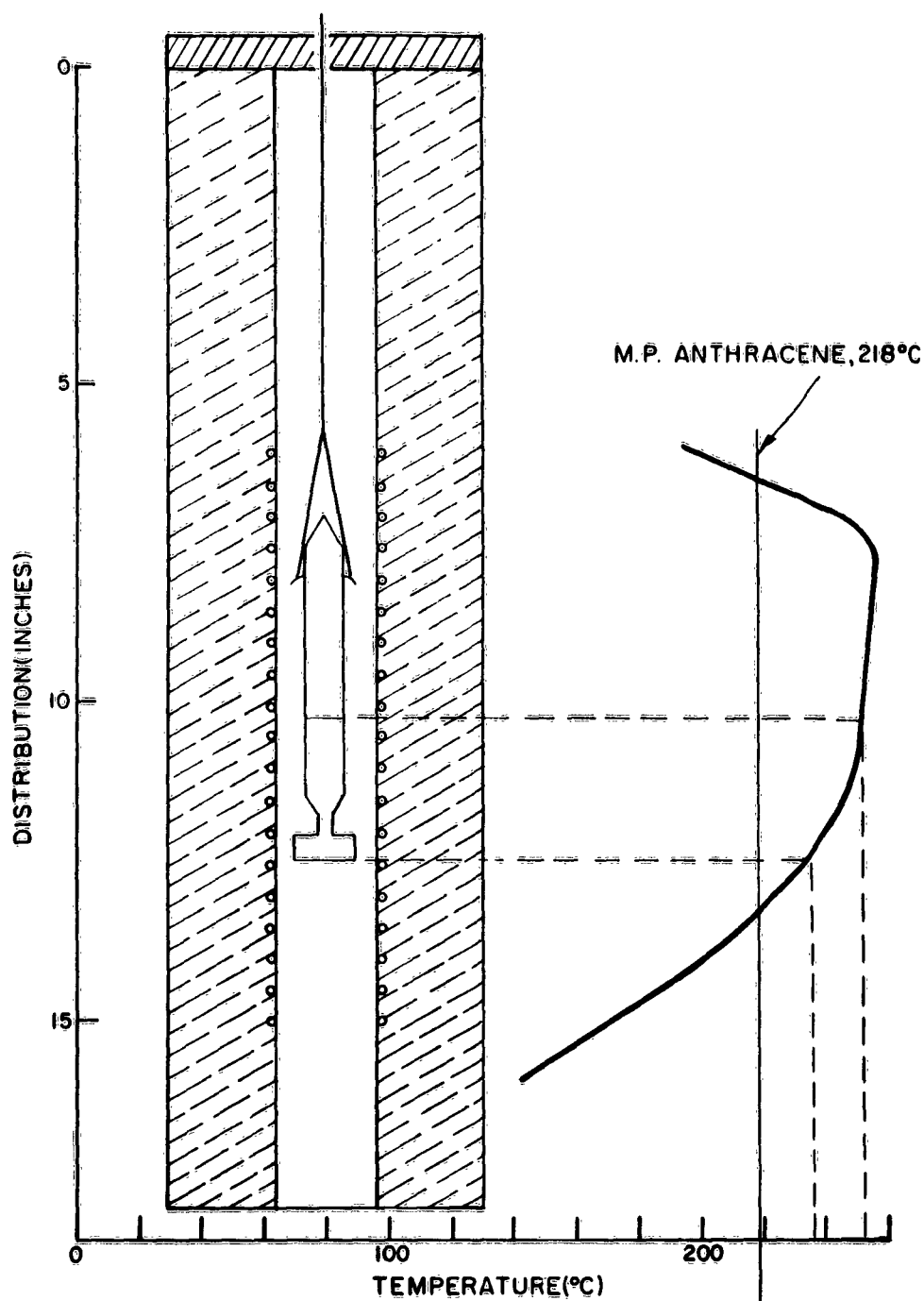
M.P. ANTHRACENE, 218°C

FIG. VII-3

56

REFERENCES

1. H. Kallmann and M. Pope, J. Chem. Phys. **32**, 300 (1960).
2. H. Kallmann and M. Pope, Nature **186**, 31 (1960).
3. P. Mark and W. Helfrich, J. Appl. Phys. **33**, 205 (1962).
4. T. S. Moss, "Optical Properties of Semi-Conductors," Butterworth's, London, 1961, pp. 83, 156, 212.
5. M. A. Lampert, Proc. I.R.E. **50**, 1781 (1962).
6. W. Helfrich and P. Mark, Z. Physik **166**, 370 (1962).
7. A. Many and G. Rakavy, Phys. Rev. **126**, 1980 (1962).
8. R. G. Kepler, Phys. Rev. **119**, 1226 (1960).
9. H. Feilchenfeld and A. Many, paper presented at Organic Crystal Symposium, National Research Council of Canada, Ottawa, Oct. 10-12, 1962.
10. F. J. Morin, Phys. Rev. **93**, 1195, 1199 (1954).
11. R. A. Keller and H. E. Rast, J. Chem. Phys. **36**, 2640 (1962).
12. L. Friedman, Thesis, University of Pittsburgh, 1961. Also U.S.A.F. Contract # AF49(638)-323.
13. G. Heilmeier, G. Warfield and S. Harrison, Phys. Rev. Letters **8**, 309 (1962).
14. C. Herring, J. Appl. Phys. **31**, 1939 (1960).
15. K. W. Plessner, Proc. Phys. Soc. **B64**, 671 (1951) and H. W. Henkels, J. Appl. Phys. **22**, 916 (1951).
16. J. Dresner, J. Chem. Phys. **35**, 1628 (1961).
17. W. E. Spear, Proc. Phys. Soc. **B76**, 826 (1960).
18. H. P. D. Lanyon and W. E. Spear, Proc. Phys. Soc. **B77**, 1157 (1961).
19. H. Gobrecht and A. Tausend, Z. Physik **161**, 205 (1961).
20. A. Rose, RCA Rev. **12**, 362 (1951).
21. H. W. Henkels and J. Maczuk, Phys. Rev. **91**, 1562 (1953) and J. Appl. Phys. **24**, 1056 (1953).
22. P. K. Weimer and A. D. Cope, RCA Rev. **12**, 314 (1951).
23. J. Dresner, unpublished work.
24. R. W. Smith and A. Rose, Phys. Rev. **97**, 1531 (1955).
25. W. Ruppel, Helv. Phys. Acta **31**, 311 (1958).
26. A. Many, M. Simhony, S. Z. Weisz and J. Levinson, J. Phys. Chem. Sol. **22**, 1628 (1961).
27. N. F. Mott and R. W. Gurney, "Electronic Processes in Ionic Crystals," Oxford University Press, New York, 1940, 1st ed., p. 172.

REFERENCES (Continued)

28. A. Rose, Phys. Rev. **97**, 1538 (1955).
29. M. Silver, P. Mark, D. Olness, W. Helfrich and R. C. Jarnigan, J. Appl. Phys. **33**, 2988 (1962).
30. A. Many, to be published.
31. The information presented in this introduction was abstracted from references 32, 33, and 35 which are publications of the duPont group as well as from unpublished literature (reference 34) furnished to us by duPont.
32. D. S. Acker, et. al., J. Am. Chem. Soc. **82**, 6408 (1960).
33. Chemical and Engineering News **39**, 42 (Jan. 9, 1960).
34. Unpublished information from the duPont Laboratories.
35. R. G. Kepler, P. E. Bierstedt and R. E. Merrifield, Phys. Rev. Letters **5**, 503 (1960).
36. W. Helfrich and P. Mark, Z. Physik **168**, 495 (1962).
37. H. Boroffka, Z. Physik **160**, 93 (1960).
38. W. P. Dyke, J. K. Trolan, W. W. Dolan and G. Barnes, J. Appl. Phys. **24**, 570 (1953).
39. H. K. Henisch, "Rectifying Semi-Conductor Contacts," Oxford University Press, London, 1957, Ch. V, pp. 123-149.
40. W. Shockley, "Electrons and Hole in Semiconductors," D. van Nostrand Company, New York, 1950 pp. 86-95, 108-114.
41. O. H. LeBlanc, Jr., J. Chem. Phys. **35**, 1275 (1961).
42. R. A. Smith, "Semiconductors," Cambridge University Press, New York, 1959, pp. 170-176.
43. M. A. Lampert, Phys. Rev. **103**, 1648 (1956).
44. R. H. Parmenter and W. Ruppel J. Appl. Phys. **30**, 1548 (1959).
45. W. O. Milligan, J. Phys. Chem **38**, 797 (1934).
46. E. S. Rittner and J. H. Schulman, J. Phys. Chem. **47**, 537 (1943).
47. Analysis for Cd by S. J. Adler and B. L. Goydish; S, C, and H analysis by Schwarzkopf Microanalytical Laboratory, Woodside, New York.
48. R. H. Bube and A. B. Dreeben, Phys. Rev. **115**, 1578 (1959).
49. R. H. Bube, J. Appl. Phys. **31**, 2239 (1960).
50. R. H. Bube, E. L. Lind and A. B. Dreeben, Phys. Rev. Letters **9**, #4 p. A4, abstract of Phys. Rev. (Aug. 15, 1962).
51. R. C. Brasted, "Comparative Inorganic Chemistry," D. van Nostrand Company, Princeton, New Jersey, 1961, Vol. 8.
52. L. M. Nijland, Philips Res. Rep. **9**, 259 (1954).
53. T. Sato and H. Kaneko, Technology Rep. Tohoku Univ. **14**, 45 (1950) and **15**, 1 (1950).

REFERENCES (Continued)

54. R. A. Hyman, Proc. Phys. Soc. B69, 743 (1956).

55. P. T. Kozgrev, Sov. Phys. Tech. Phys. 3, 470 (1958) (Eng. Trans.).

56. R. A. Hyman, Proc. Phys. Soc. B69, 771 (1956).

57. J. Ferguson and W. G. Schneider, Can. J. Chem. 36, 1633 (1958).

58. P. Mark, Z. Naturforsch. 16, 950 (1961).

59. H. Kallmann and M. Pope, Rev. Sci. Inst. 29, 993 (1958).

60. F. R. Lipsett, Can. J. Phys. 35, 284 (1957).